Acta Geotechnica
https://doi.org/10.1007/s11440-020-01057-w

RESEARCH PAPER

3D modelling of strip reinforced MSE walls

I. P. Damians[1,3] · R. J. Bathurst[2] · S. Olivella[1,3] · A. Lloret[1] · A. Josa[1]

Received: 1 March 2020 / Accepted: 11 August 2020

Abstract

This paper reports the results of 3D numerical modelling of a 6-m-high mechanically stabilised earth (MSE) wall constructed with concrete panels and steel or polymeric strip reinforcement. These systems pose numerical challenges as a result of the discontinuous reinforcement arrangement which is not the case for MSE walls constructed with continuous reinforcement layer configurations. Details of the numerical approach including modelling of the reinforcement strips, concrete facing panels and compressible bearing pads between panels are described. Examples of numerical predictions for facing deformations, toe loads due to soil down-drag behind the panels, soil and reinforcement settlements, and reinforcement tensile loads are presented. The influence of reinforcement stiffness is demonstrated by comparing numerical predictions for the same MSE wall with relatively inextensible steel strips and with relatively extensible polymeric strips. Of particular interest are the results showing the disruption of earth pressures along vertical and horizontal planes in the reinforced soil zone as a result of the discontinuous strip inclusions, and the vertical load that accumulates on the reinforcement strips close to the connections due to soil settlement behind the facing. The details of the modelling approach used here and the lessons learned provide a benchmark for future similar lines of investigation and for practitioners, particularly as the computational power of desktop computers continues to increase.

Keywords 3D modelling · Finite element modelling · Mechanically stabilised earth (MSE) walls · Polymeric strip reinforcement · Soil retaining walls · Steel strip reinforcement

Electronic supplementary material The online version of this article (https://doi.org/10.1007/s11440-020-01057-w) contains supplementary material, which is available to authorized users.

✉ R. J. Bathurst
bathurstrichard@gmail.com

I. P. Damians
ivan.puig@upc.edu

S. Olivella
sebastia.olivella@upc.edu

A. Lloret
antonio.lloret@upc.edu

A. Josa
alejandro.josa@upc.edu

1 Department of Civil and Environmental Engineering, School of Civil Engineering, Universitat Politècnica de Catalunya-BarcelonaTech (UPC), Barcelona, Spain

2 GeoEngineering Centre at Queen's-RMC, Civil Engineering Department, Royal Military College of Canada, Kingston, ON K7K 7B4, Canada

3 International Center for Numerical Methods in Engineering (CIMNE), Universitat Politècnica de Catalunya-BarcelonaTech (UPC), Barcelona, Spain

1 Introduction

Mechanically stabilised earth (MSE) walls constructed with incremental concrete facing panels and discontinuous strip reinforcement elements are a well-established technology. The soil–reinforcement elements most often take the form of steel strips, steel grids or polymeric strips. Other systems use steel rod and anchor arrangements. This paper is focused on strip-type soil reinforced soil walls. The internal stability design of these structures is most often based on limit equilibrium methods with empirical adjustments applied to familiar concepts of earth pressure theory. The most common limit states for internal stability are reinforcement pullout, reinforcement rupture and connection failure between the soil–reinforcement and wall facing units. For MSE walls constructed with continuous reinforcement layers in the running wall face direction, 2D (plane strain) analyses are appropriate. Examples are walls constructed with continuous sheets of geogrid, geotextile and steel grids (bar mats and welded wire). For discontinuous reinforcement systems, 2D limit equilibrium-based analyses are useful approximations suitable for design of routine wall structures for ultimate (failure) limit states (e.g. [1, 11, 18]). Nevertheless, these approaches cannot be used to explicitly predict performance features related to wall deformations for discontinuous and continuous reinforcement cases because they are force based. The challenge to model walls under operational (working stress) conditions is greater for discontinuous reinforcement material cases than for continuous sheet-like reinforcement arrangements. Ideally, 3D numerical modelling using the finite element method (FEM) and finite difference method (FDM) is best suited for this purpose.

The objective of the current study was to develop a 3D FEM model to simulate the construction and end-of-construction performance of a typical concrete panel MSE wall of height $H = 6$ m constructed with steel strips and with soil materials having a range of properties. The width of the model is 1 m corresponding to the repeating unit of the wall (i.e. width of one-half panel).

The model geometry for the reinforced zone and panels in this study is typical of actual structures. However, rather than matching the material properties for the component materials, interfaces and foundation to a particular constructed wall structure, values were selected from prior 2D modelling of walls reported in the literature and the experience of the writers and co-workers with 2D modelling of other MSE walls (e.g. [19, 21, 23, 49, 50]).

The incremental construction of the wall was simulated in the numerical modelling. Performance results at end of construction for wall displacements, reinforcement loads, and horizontal and vertical earth pressures are reported. The base case for the current investigation is a steel strip MSE wall. Sensitivity analyses were carried out to investigate the influence on wall performance of different properties assigned to the backfill soil, foundation soil, the horizontal bearing pads located between panels, stiffness of the strip reinforcement (e.g. more extensible polymeric strips), and soil–facing and soil–strip interfaces.

This study is the first to model a tall (6-m-high) MSE soil wall using a 3D FEM approach with discrete strip reinforcement inclusions having very different stiffness and a range of other component model properties. The details of the modelling approach used here and the lessons learned provide a benchmark for future similar lines of investigation, particularly as computational power of desktop computers continues to increase.

2 Prior related work

Examples of numerical 2D FEM modelling of MSE walls with *continuous* reinforcement layers and different types of hard concrete facing can be found in the literature. These include the work of Cai and Bathurst [12], Karpurapu and Bathurst [32], Rowe and Ho [42], Rowe and Skinner [43], Yoo et al. [48], and Ling and Leshchinsky [34], amongst many others. Similar attempts using the finite difference method (FDM) can be found in the papers by Hatami and Bathurst [26, 27], Huang et al. [29], Damians et al. [20] and Yu et al. [49]. Many of these papers have demonstrated satisfactory predictions of important measured performance features of instrumented full-scale walls in the field and in the laboratory.

2D numerical models using FEM and FDM approaches have been used to simulate the performance of hard face concrete walls constructed with *discontinuous* steel and polymeric strip reinforcement (e.g. [2, 9, 13, 17, 19, 21, 23, 49, 53]), and steel anchors [46]. However, in these studies it was necessary to convert the discrete reinforcing strips to equivalent continuous layers.

The modelling of MSE walls with discontinuous reinforcing elements using a 2D model has been recognised as an imperfect approach because the distribution of soil stresses in the cross-plane direction is interrupted by the reinforcement inclusions [38].

3D finite element modelling of MSE walls with continuous geosynthetic reinforcement can been found in the literature (e.g. [47, 24]). However, the 3D models were required to account for the 3D problem geometry and discontinuous surface loading. The reinforcement layers were modelled as planar sheets.

Ho and Smith [28] report an early attempt at true 3D modelling of the steel strips in a reinforced soil wall. They used brick elements to model the repeating column of soil, reinforcement and the facing panels, and a second adjacent column of elements to model the uninterrupted soil. The width of the reinforced soil column matched one-half the reinforcement width, and the two columns together had a width equal to one-half the horizontal spacing between reinforcement inclusions. Contours of shear stresses were very different at vertical surfaces taken though the middle of the reinforcement strips and parallel surfaces taken through the intermediate unreinforced soil zone.

Bourgeois et al. [9] used a homogenisation approach to account for the discrete reinforcement strips and the soil in a 3D FEM simulation of a steel strip reinforced wall of height 5.74 m supporting an embankment for a railway track simulated by a pair of footings. Their finite element mesh comprised of 5000 nodes and 2000 elements. The same team carried out a 3D FEM simulation of the same problem by using 50,000 nodes and modelling the reinforcement strips with "friction bar elements" developed specially for the FEM program used to carry out the simulations [10]. The latter work is the closest related study to the current investigation. However, the general approach and the scope of their paper and the current study are very different.

3 Numerical approach

3.1 General

The computer software program CODE_BRIGHT [14, 39] was used to carry out the numerical simulations in this study. This program was used because it is freely available, is familiar to the writers and can accommodate large 3D geomechanics problems. It has a number of advanced constitutive models available in the software library. However, simple models described later were adopted in the current study. The calculations were performed in small strain mode to keep simulation runtimes manageable. Regardless, the objective of the numerical modelling was to investigate wall performance under working stress conditions consistent with the notion of small strain deformations.

3.2 Finite element model

Figure 1 gives an overview of the 3D model and wall components. The model geometry for the reinforced zone and panels captures the principal features of a typical steel strip reinforced soil wall while adopting simple geometry and boundary conditions to ensure that computational demands were not excessive. The properties of the component materials and interfaces are taken from prior related 2D modelling of MSE walls by the writers and co-workers as explained later.

The numerical slice represents an idealised 1-m wide repeating unit in the direction of the running length of the wall with panels 1.5 m high. The steel reinforcement strips are taken as 50 mm wide by 4 mm thick and placed at vertical spacing of 0.75 m; these are typical dimensions for these systems (e.g. [25, 45]).

The numerical model represents a 6-m-high wall with four panels. The length of the reinforced zone is about $L = 4.2$ m which is $0.7H$ where H is the wall height. A ratio of $L/H = 0.7$ is a typical recommended value for design (e.g. [1]). The numerical simulations did not include any surcharge at the top boundary of the model.

Figure 2 shows mesh and material property zones for the panels, reinforcement and connections. Careful attention was paid to the bearing pad zone dimensions and assignment of properties because previous numerical modelling by the writers has shown that these details have a critical influence on facing behaviour for these types of walls (e.g. [19]). The figure shows that the steel strip layer is 50 mm wide by 5 mm thick. The 5 mm dimension was selected to facilitate an optimum level of mesh discretisation. However, the properties for the base case steel strip models in this study were adjusted (Eq. 1) to match steel strips that are 4 mm thick and placed at typical 0.75 m horizontal centre-to-centre spacing between strips in each reinforcement layer [2]. Hence, for base case calculations using a 1 m horizontal spacing, the reduced equivalent elastic modulus of the steel (per unit running length of wall) (E_{eq}) was computed to give the same stiffness of $J_r = 56$ MN/m for a 4-mm-thick steel strip as follows:

$$E_{eq} = \frac{J_r}{A_{r,3D}} = 224 \text{ GPa/m} \quad (1)$$

where $A_{r,3D}$ is the reinforcement cross-sectional area of the model (i.e. $A_{r,3D}$ = 50 mm wide × 5 mm thick = 2.5×10^{-4} m^2) and J_r is the axial reinforcement stiffness per running metre of wall, calculated as:

$$J_r = (EA)_r \left(\frac{n_r}{L_p}\right) = 56 \text{ MN/m} \quad (2)$$

where $(EA)_r$ is the true reinforcement axial stiffness (i.e. elastic modulus of the reinforcement ($E_r \simeq 210$ GPa) times the cross-sectional area of the reinforcement (A_r = 50 mm wide × 4 mm thick = 2.0×10^{-4} m^2) matching the steel strips reported by Abdelouhab et al. [2]; n_r is the number of reinforcement strips per panel ($n_r = 2$); and L_p is the length of a panel (1.5 m). Thus, n_r/L_p corresponds to the horizontal centre-to-centre spacing between reinforcement strips of 0.75 m.

Figure 1b shows small elements with softer material (elastic modulus = 0.1 MPa) that were introduced in the numerical mesh at the end of the reinforcement to prevent the development of a numerical hard spot that can act as an anchor and therefore artificially over-stiffen the reinforced soil zone. The width and height of each element are 150 mm and 105 mm (Fig. 2b) and occupy the last 100 mm at the free end of the reinforcement.

All elements in the finite element mesh were 8-noded hexahedra including zones used to simulate the interfaces between dissimilar materials. The finite element mesh was composed of 12,318 elements with 13,800 nodes.

The bottom domain boundary was fixed in numerical simulations. The foundation boundary at 4.5 m below the wall was judged to be far enough away not to influence numerical outcomes in any practical way. The vertical y–z boundaries were fixed in the cross-plane (x) direction. Hence, the soil and panel y–z boundaries in the vertical (y) direction were free to move. The domain boundaries at the front of the foundation zone and at the back of foundation and retained fill zones were free to move in the vertical direction. The distance of the wall facing from the back boundary of the domain (8.2 m in Fig. 1) was selected as a practical compromise to minimise far-field boundary effects on wall facing deformations and computation time. Furthermore, the length of the retained fill is large enough to contain a potential active wedge

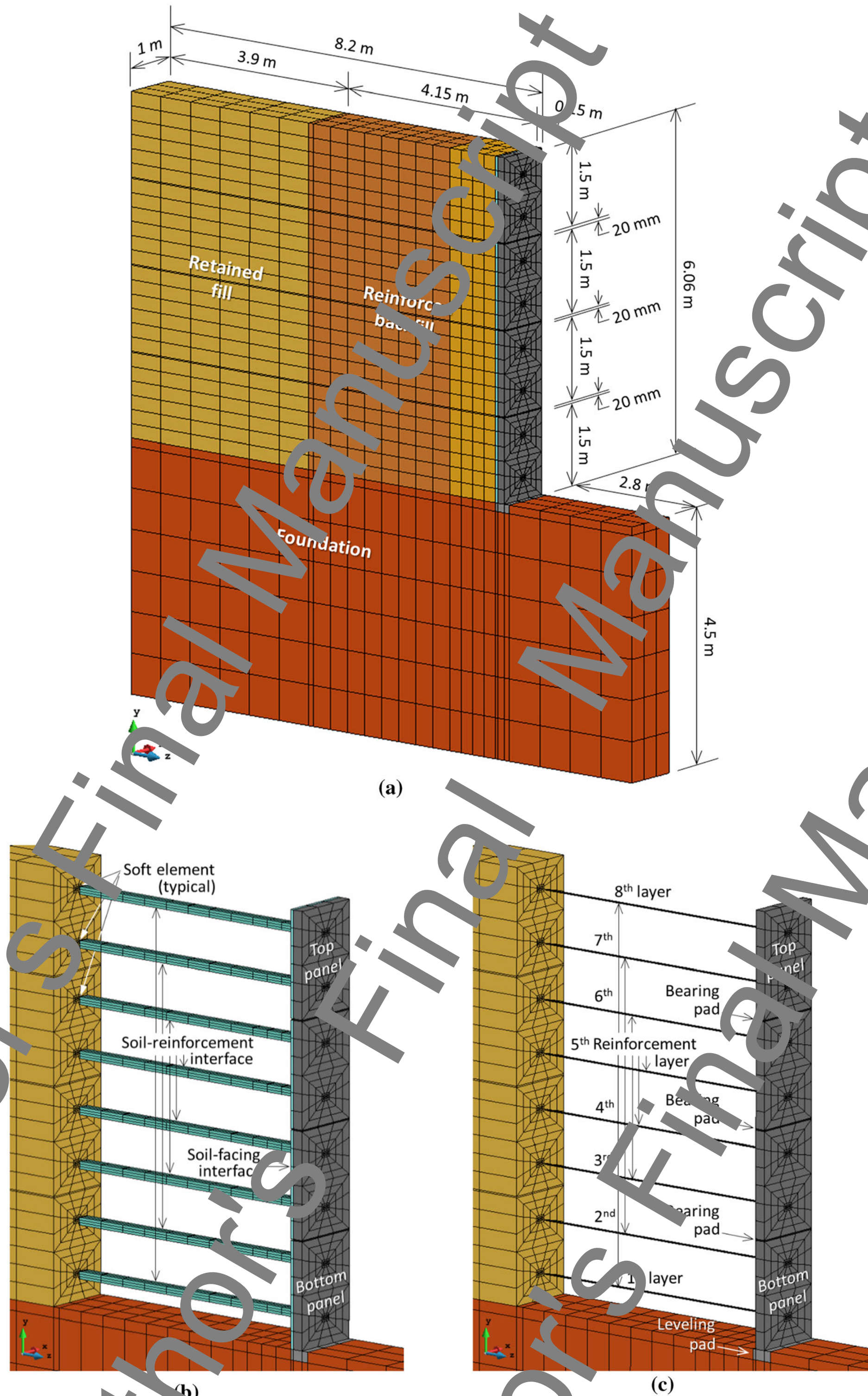

Fig. 1 3D model overview: **a** finite element mesh and main dimensions for vertical repeating slice, **b** interfaces and **c** structural components

propagating from the heel of the reinforced backfill zone. The qualitative performance of the wall using a more distant back boundary is expected to remain unchanged, and any quantitative differences are judged not to be of practical importance. This is because it is the foundation soil and the near field behind the facing that strongly influence facing deformations.

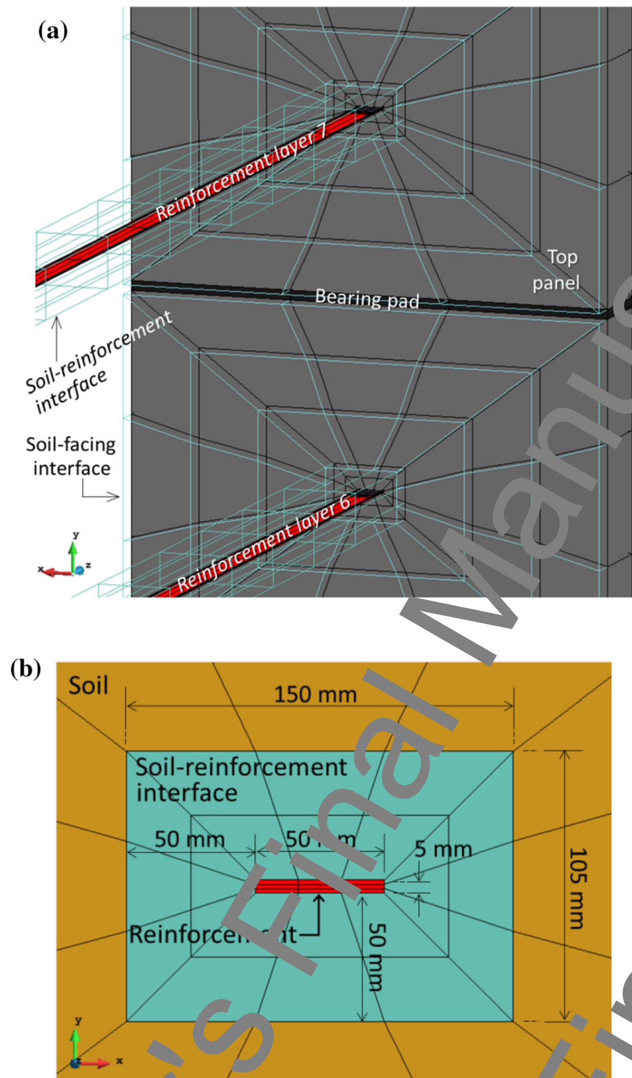

Fig. 2 Mesh and material property zones for the panels, reinforcement and connections: **a** facing panel joint and reinforcement connections, and **b** vertical slice through reinforcement strip showing soil interface zone

The numerical model was constructed in stages. The foundation zone was turned on first. Then the first panel was placed together with the concrete levelling pad. This panel was restrained horizontally to simulate the panel braces that are used to temporarily support the panels in the field. The soil layers and reinforcement layers were then placed in two steps. The second panel was placed and braced after the first 0.75 m of soil was in place. Once all the soil behind the second panel was in place, the support for the bottom panel was removed. The same staged construction was repeated for the remaining panel units as illustrated in Figure S1 in the Supplemental Material for this paper.

Compaction of the soil layers was not simulated directly in this study. However, the reinforced backfill soil located within the first 1 m beyond the wall face was assigned a lower modulus value than the remainder of the reinforced zone as explained in the next section.

Simulations were performed on a PC using one Intel(R) Core(TM) i7-8850H CPU processor running at 4.30 GHz (maximum turbo frequency) and with 32 GB of RAM memory. The elapsed CPU time for the cases in this study varied from 20 to 50 h.

3.3 Material properties

3.3.1 Base case

As noted earlier, the base case for the numerical modelling in this study is the 6-m-high wall reinforced with steel strips shown in Fig. 1. Material types and properties used in this study are summarised in Tables 1, 2, 3 and 4. The material properties used in the base case analysis are shown in the shaded cells of Table 4.

Allen and Bathurst [5] have demonstrated that wall performance is sensitive to reinforcement global stiffness (S_g) which is computed as the sum of reinforcement stiffness (J_r) from all reinforcement layers divided by wall height (H). For example, wall reinforcement loads will increase with greater global reinforcement stiffness when all other properties remain unchanged. The value of S_g was computed as 42 MPa (Table 4) which falls within the range of 30–400 MPa reported by Allen and Bathurst [5, 6] based on data taken from 24 full-scale instrumented steel strip reinforced soil walls under operational conditions. These walls were judged to fall within the inextensible reinforcement category. The maximum steel strip reinforcement strains for all cases and layers in the current study were less than 0.03%, which is well below the yield strain of 0.2% for the steel. For comparison, a monitored 17-m-high production steel strip wall described by Runser et al. [45] recorded strains up to 0.08% at end of construction. The computed maximum strains for the polymeric straps in this paper were about 0.2% which is at the low end of values measured in actual PET strap walls and is well below 1% strain that is recommended to keep these systems at working stress levels [36] and to ensure adequate margins of safety against tensile failure [8].

All soil materials were assumed to be linear elastic–plastic. The soils are granular type with shear strength best described by peak plane strain friction angles. Plane strain friction angles of a granular soil can be determined from a "plane strain" test apparatus that confines a block of soil between two frictionless parallel plates that prevent out-of-plane deformations at the plate boundaries. Hence, this test apparatus constrains the soil similar to the y–z boundaries in the numerical model used in this study. Peak friction angles computed from plain strain tests for dense granular

Table 1 Soil material properties for base case taken from Yu et al. [49]

Parameter	Soil material		
	Backfill[a]		Foundation
	(> 1.0 m from face)[b]	(< 1.0 m from face)	
Unit weight, γ_n (kN/m^3)	18		20
Elastic modulus, E (MPa)	20	10	45[c]
Poisson's ratio, v (−)	0.3		0.3
Cohesion, c (kPa)	1		5
Friction angle, ϕ (°)	44		36
Dilatancy angle, ψ (°)	14		6

[a]Includes both reinforced and retained soil materials

[b]Retained fill assumed to have the same strength–stiffness soil properties as the reinforced soil zone beyond 1.0 m from facing

[c]Larger elastic modulus selected to give the foundation zone the same vertical stiffness as the wall backfill soil

Table 2 Non-soil material properties for base case

Parameter	Material				
	Reinforcement		Concrete		Bearing pads (HDPE)
	Steel strip	Polymeric strap			
Unit weight, γ_n (kN/m^3)	75	7.5	24		10
Elastic modulus, E (MPa)	210,000	5000 and 500	32,000	Panels	3.2[b]
			25,000	Levelling pad	
Poisson's ratio, v (−)	0.3	0.3	0.2		0.01[c]

[a]Strips are 50 mm wide and 4 mm thick and placed at horizontal spacing of 0.75 m. The steel used in the numerical simulations to give the same stiffness using a 5 mm thick strip J = 56 MN/m

[b]Equivalent modulus of horizontal joint material for 1-m running length of wall based on two HDPE bearing pads placed at 1.5 m intervals for a typical physical wall [16, 23]

[c]Negligible Poisson's ratio value to account for internal spaces (voids) and ribbed geometry which reduces lateral expansion of each pad under vertical compression

Table 3 Interface material properties for base case (data from [49])

Parameter	Interface	
	Soil–facing[a]	Soil–reinforcement
Unit weight, γ_n (kN/m^3)	19	19
Elastic stiffness modulus, E (MPa)	4.02	20
Poisson's ratio, v (−)	0.45	0.45
Cohesion, c (kPa)	0.6	1
Friction angle, δ (°)	30.1	26.6[b]
Dilatancy angle, ψ (°)	0	14[c]

[a]Soil–facing interface strength–stiffness reduction factor assumed equal to R_i = 0.6, which influences both stiffness and strength ([21])

[b]Soil–reinforcement steel strip interaction assuming δ = 26.6° (= ϕ_i) is equivalent to an interface reduction factor of R_i = tan δ/tan ϕ = 0.52, which corresponds to a pullout friction factor F^* = tan δ = tan (26.6°) = 0.50 (i.e. F^* = tan δ = R_i tan ϕ = 0.52 tan(38°) = 0.40). The base case F^* = 0.4 in the current study and matches AASHTO [1] specifications for smooth steel strips but is low for ribbed steel strips and polymeric strips [37]. This value is assumed to remain constant at reinforcement locations deeper than 3 m from top of wall (i.e. all reinforcement layers modelled), which is in good agreement with results of Chida and Nakagawa [15] and numerical results reported by Yu et al. [49]. According to FHWA [25], the friction angle of the soil to compute F^* is based on the peak friction angle from triaxial or direct shear tests

[c]Assumed equal to backfill soil dilatancy angle for soil–reinforcement interface material zone

soils are larger than values deduced from triaxial tests. Using the relationship proposed by Kulhawy and Mayne [33], the peak plane strain friction angle of 44° corresponds to 38° from triaxial tests. This value is typical for high quality granular fill materials that are recommended in AASHTO [1] specifications for MSE walls. A value of cohesion $c = 1$ kPa was selected to ensure numerical stability at the soil zone (top) free boundaries during construction (e.g. [19]). The elastic modulus of the soil located within 1 m of the back of the wall facing was reduced by 50% to capture the effect of lower compaction energy in this region when lighter compaction equipment is used directly behind the facing as recommended for good construction practice [25]. This reduced soil modulus technique for this zone has been used in 2D simulations of other MSE walls for the same reason given here (e.g. [19, 49]).

The modulus and friction angle properties of the interfaces were related to the adjacent soil using the reduction factor (R_i). This value was set to 0.6 for the facing–soil interface and 0.52 for the soil–reinforcement interface. The facing–soil interface was assumed to be smooth and thus non-dilatant while the soil–reinforcement interface was assumed to be rough and therefore was assigned the same dilatancy angle as the adjacent soil. The choice of soil and interface parameters used here was based on experience from 2D modelling of steel strip reinforced walls by Damians et al. [21] and Yu et al. [50]. The friction coefficient for the base case was assumed as $F^* = 0.4$ which is at the low end for polymeric strips [2, 35, 36] and a conservative (safe) estimate for design with ribbed steel strips [1].

The mechanical properties of the horizontal joint between adjacent panels were selected to transform the bearing pads that are constructed with internal voids and ribbed geometry to a continuous thin solid rectangular strip zone with equivalent one-dimensional compressive stiffness (E_p). The joint material for base case models is equivalent to a row of bearing pads manufactured from high density polyethylene (HDPE) [23].

3.3.2 Additional cases and material properties for sensitivity analyses

Parametric analyses were carried out in this study to examine the influence of a range of soil and material properties on numerical modelling outcomes. Nine additional numerical simulations were carried out using the combinations of values shown in Table 4. Included in the parametric analyses were cases with polymeric strips that were assigned tensile stiffness values of $J_r = 1.25$ and 0.125 MN/m (load per m width of strap). These values are at the top and bottom range of secant stiffness values computed at 1000 h and 2% strain from constant load tests [7]. The corresponding global reinforcement stiffness values are $S_g = 1.7$ and 0.17 MPa, respectively. The higher stiffness case is in agreement with eight instrumented field walls examined by Miyata et al. [36] that were constructed with modern polymeric (PET) strips and shown to have S_g values in the range of 1.96–0.79 MPa. The lower value in the current study falls below the field cases noted above but was selected in one set of analyses to explore the influence of reinforcement stiffness on numerical outcomes. Allen and Bathurst [6] showed that walls constructed with other types of relatively *extensible* polymeric reinforcement products (i.e. geogrids and geotextiles) can also be expected to have $S_g \leq 2$ including values that are less than $S_g = 0.17$ MPa in the current study.

Analyses were also carried out with different backfill and foundation modulus values (E_b and E_f) and a more compressible bearing pad arrangement. Numerical simulations were repeated with a lower interface strength and stiffness reduction factor (R_i). Finally, calculations with different soil–reinforcement pullout friction factor F^* assigned to each reinforcement layer were performed. Based on AASHTO [1] recommendations, the layers for ribbed steel strips were assigned values of F^* linearly interpolated between 0.80 at the bottom of the wall and 2.0 at the top of the wall.

4 Model approach applied to PWRI wall case study

Many of the baseline model parameters were taken from the paper by Yu et al. [49] who modelled the instrumented steel strip wall constructed at the Public Works Research Institute (PWRI) in Japan and reported by Chida and Nakagaki [15]. In order to develop confidence with the 3D model developed for this study, the measured and numerically predicted reinforcement loads and wall toe load from the earlier study by the writers and co-workers were revisited [49]. The material properties for the PWRI wall numerical analysis are identified in the tables presented earlier. It should be noted that the PWRI wall was a test wall supporting a narrow embankment with an inclined surcharge and was constructed with cruciform shape facing panels. Hence, the general arrangement was more complicated than the 3D wall slice that is the focus of the current study.

Figure 3 shows the measured reinforcement loads together with predictions using the same CODE_BRIGHT 3D FEM code as in the current study (i.e. using a 3D analysis) and two other commercial 2D numerical modelling codes (FEM - [40, 41]; FDM - FLAC- [30]). The 3D numerical and measured results are judged to be in

Table 4 Parameter values for base case and sensitivity analyses

Case	Backfill stiffness E_b (MPa)		Foundation stiffness E_f (MPa)	Bearing pad layer stiffness E_p (MPa)	Reinforcement stiffness [(b)] J_r (MN/m)	Global reinforcement stiffness $S_g = \Sigma J_r/H$ (MPa)	Soil-facing interface [(c)]			Soil-reinforcement pullout friction factor F^* (-)
	(> 1 m)	< 1 m)					Strength-stiffness reduction factor R_i (-)	Stiffness E_{if} (MPa)	Friction angle δ (°)	
0 [(a)]	20	10	45	3.3	56.0	42	0.6	4.0	30	0.4
1	10	5	4.5	3.3	56.0	42	0.6	4.0	30	0.4
2	10	5	45	3.3	56.0	42	0.6	4.0	30	0.4
3	100	50	4.5	3.3	56.0	42	0.6	4.0	30	0.4
4	100	50	450	3.3	56.0	42	0.6	4.0	30	0.4
5	20	10	45	0.4 [(d)]	56.0	42	0.6	4.0	30	0.4
6 [(e)]	20 & 50	10 & 25	13.5	0.4 [(d)]	68.2	90.9	0.6	10.0	30	0.6 to 1.8
7a [(f)]	20	10	45	3.3	1.25	1.7	0.6	4.0	30	0.5
7b [(g)]	20	10	45	3.3	0.125	0.17	0.6	4.0	30	0.5
8	20	10	45	3.3	56.0	42	0.3	1.0	16	0.4
9	20	10	45	3.3	56.0	42	0.6	4.0	30	0.8 to 2.0 [(h)]

[a]Base case values are shown in shaded cells

[b]Stiffness based on 1-m running length of the wall with reinforcement strips placed at horizontal spacing of 1 m

[c]Interface reduction factor is multiplied with shear modulus of adjacent soil to compute shear modulus of interface elements. The equivalent calculation using E and ν of the adjacent soil is: $E_i = 1.45 (R_i)^2 (E/(1+\nu))$ ([22]). Interface reduction factor is multiplied with soil friction coefficient to compute interface element friction angle as: $\delta = \text{atan}(R_i \tan\phi)$

[d]EPDM bearing pads [19, 23]

[e]Values from Yu et al. [49] for PWRI wall case [15]. Wall constructed with smooth steel strips

[f]Stiffness is at top end of range for polymeric (PET) strip reinforcement [36]

[g]Stiffness is at lower end of range for polymeric (PET) strip reinforcement [36]

[h]AASHTO [1] for ribbed steel strips

reasonable practical agreement in the plots in Fig. 3 given the complexity of the physical system. Increasing the backfill elastic modulus from the base case value of 20 MPa to a stiffer value of 50 MPa was judged to improve the overall agreement between measured and predicted values in this study using the 3D FEM model. Also shown in the figure are the 2D numerical model results reported by Yu et al. [49] using the program FLAC and 2D modelling by the writers using the program PLAXIS. These values also appear to do well, but the numerical outcomes vary with choice of numerical approach (i.e. FEM code or FDM). It can be concluded that the 3D model does not have practical advantage over the 2D models when comparisons are limited to tensile reinforcement loads. The disadvantage of the 2D approach is the discontinuous reinforcement strips must be treated as continuous elements in the plane strain (x) direction. This poses a challenge for steel strip walls that are constructed with variable horizontal spacing between reinforcement strips in a layer, as in the Minnow Creek wall in the USA investigated by Runser et al. [45] and Damians et al. [21].

Computed toe and foundation vertical pressures for the PWRI wall using the 3D model are presented in Fig. 4. Foundation pressures were not measured in the physical test. The measured vertical toe pressure deduced from measurements reported by Chida and Nakagaki [15] is 296 kPa, which is close to the calculated value of 309 kPa using the 3D numerical model in the current study. The toe load is greater than the self-weight of the column panels. The ratio of these values is the footing load factor computed as 2.15 and 2.06 for numerical and measured cases, respectively. The difference in toe load and panel self-

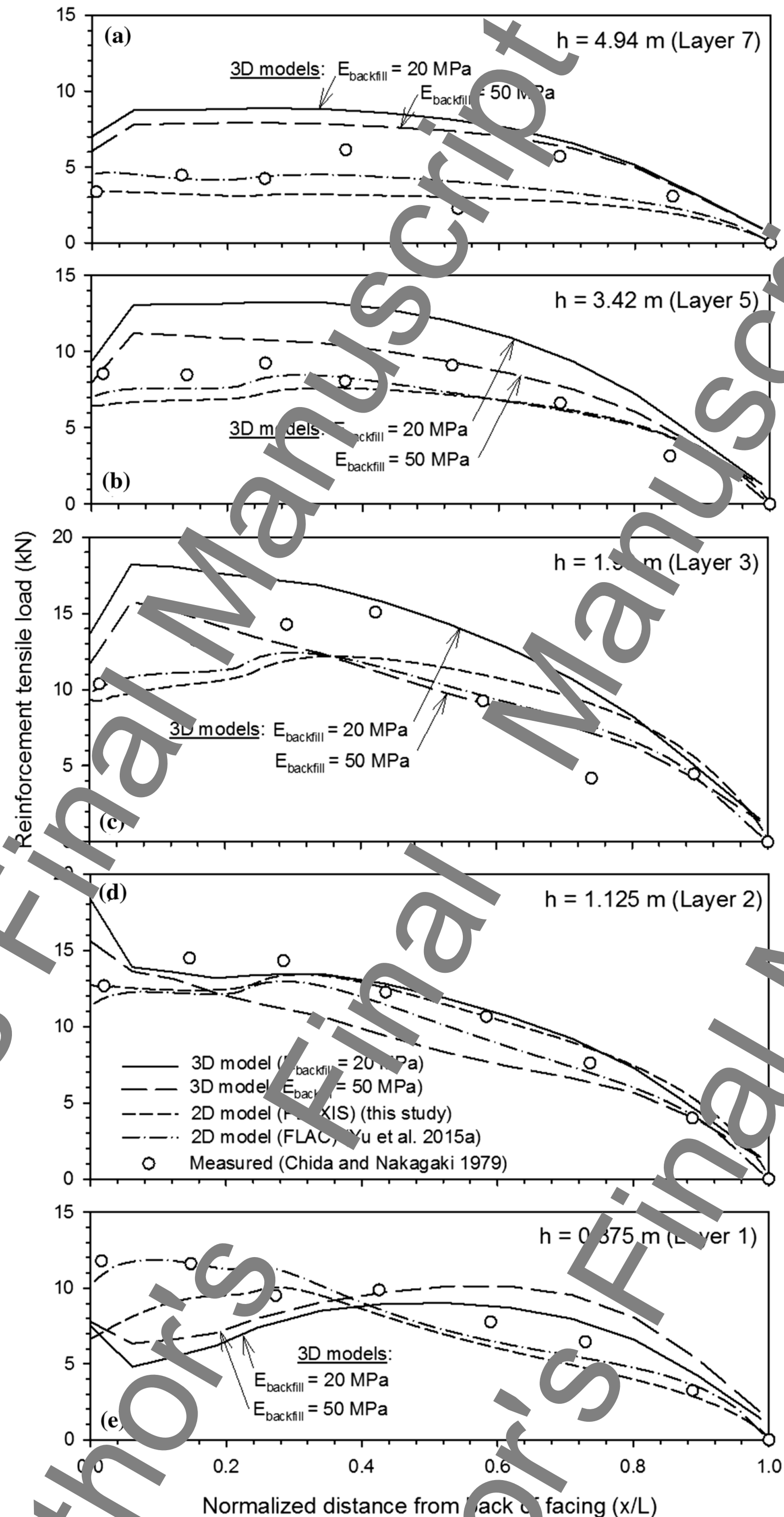

Fig. 3 Measured and predicted tensile reinforcement loads for PWRI wall in current study and numerical (FLAC) results reported by [49] using Case 6 material properties in Table 4. *Note*: *h* = height of layer above the toe of the wall

weight is ascribed to the down-drag shear stresses developed between the panels and the reinforced soil, and hanging up of the reinforced soil on the reinforcement strips as the wall panels move out and the soil behind moves down.

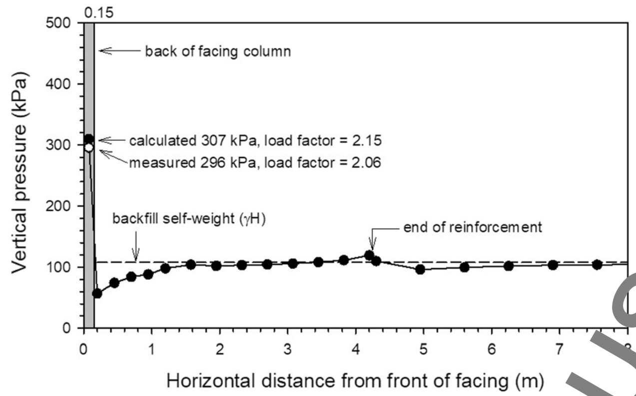

Fig. 4 Toe and foundation vertical pressures for PWRI wall

5 Results of base case numerical simulations

5.1 Example 3D plots

An important feature of the CODE_BRIGHT program is that numerical outcomes can be extracted easily and visualised using a third-party software package. Examples are shown in Fig. 5 and in Figures S1 and S2 in the Supplementary Material to this paper.

Figure 5a shows horizontal displacements in the z direction computed with respect to the location of the toe at the end of construction. The largest deformations of about 5 mm occur behind the second panel from the bottom of the wall and dissipate with distance into the reinforced soil zone. Horizontal deformations at the wall toe and reinforced soil-retained fill boundaries are about 2 mm.

Figure 5b shows vertical displacements with respect to the original toe. Vertical displacements through the height of the facing panels are about 7–8 mm and are largely due to the compressible bearing pads. Within the reinforced soil zone and retained backfill, the relative vertical deformations are about 13 mm. The relative downward deformation of the backfill soil behind the facing panels anticipates downdrag shear forces on the back of the facing panels which was mentioned earlier for the PWRI wall case and is discussed later in the paper.

5.2 Horizontal displacements

Figure 6 shows outward displacement profiles for selected wall cases at end of construction. Wall deformations are small. However, there are detectable differences in some cases that can be ascribed to the difference in magnitude of properties assigned to different wall components. For example, Fig. 6a shows that for the same walls varying only with respect to the stiffness of the bearing pads, the wall with softer (EPDM) bearing pads led to greater deformations over the top three facing units. Not unexpectedly, the walls with more extensible polymeric strap reinforcement developed greater outward deformation than the base case steel strip reinforcement case as shown in Fig. 6b. However, the difference in outward displacements for polymeric strips bracketing the range of stiffness deduced from actual polymeric (PET) strap values was not practically different. The influence of interface reduction factor (R_i = 0.6 and 0.3) was negligible as shown in Fig. 6c. Similarly, changing the magnitude of the interface friction coefficient F^* did not have a practical influence on wall facing deformations (Fig. 6d). From this observation, it may be concluded that under operational (working stress) conditions, it is the stiffness of the reinforcement that influences wall deformations rather than the interface capacity between soil and reinforcing strip.

In all cases, the outward displacements are judged to be small enough not to be of practical concern. For example, a maximum outward displacement of 5 mm for a steel reinforced soil wall of H = 6 m corresponds to a normalised outward deformation of 0.08% of the wall height. This includes the horizontal toe deformation of close to 2 mm which is thus a large portion of the maximum wall deformation. FHWA [25] provides a chart that shows that for a steel wall of height H = 6 m and reinforcement of length L = 0.7H, a first-order approximation for maximum outward deformations that may occur during construction is 24 mm (or normalised displacement of 0.4%). The same chart anticipates maximum outward deformations of 80 mm (or normalised displacement of 1.3%) for extensible reinforced soil walls but makes no specific recommendation for polymeric strap walls. The maximum numerically predicted value in this study is about 8 mm (or normalised displacement of 0.13%) for the most extensible polymeric strap wall (Case 7b). It can be concluded that the walls in this study are well within deformation limits expected of production walls at end of construction and under operational conditions.

In real-world cases, the magnitude of wall outward displacements and final wall alignment is strongly influenced by construction quality and technique. Hence, the quantitative outcomes reported here must be appreciated in relative terms. Examples of the significant influence of construction technique on facing alignment can be found in the papers by Allen and Bathurst [4] for an 11-m-high modular block wall reinforced with geogrids and a steel strip reinforced 17-m-high incremental concrete panel wall reported by Runser [44] and Runser et al. [45]. Numerical modelling of these walls by Yu et al. [52] and Damians et al. [21] was not able to explicitly account for the effects of documented construction issues in their numerical simulations. Most often the challenge during construction is to maintain the target wall facing batter by making local

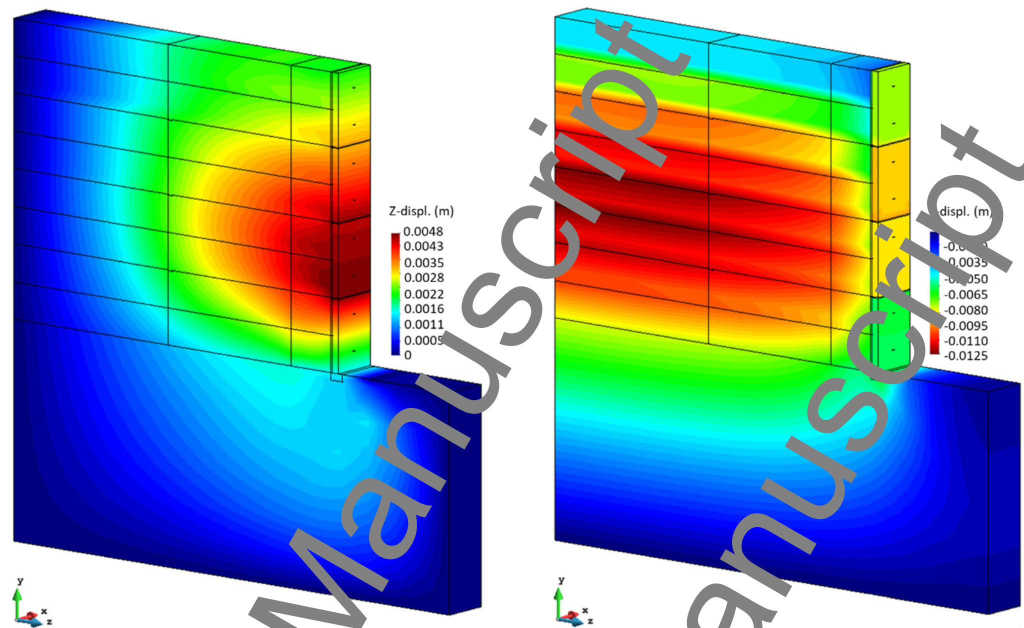

(a) horizontal displacements (m) (b) vertical displacements (m)

Fig. 5 Example plots of displacements at end of construction taken with respect to location of wall toe at start of wall construction: **a** horizontal and **b** vertical. (Case 0—steel strip wall)

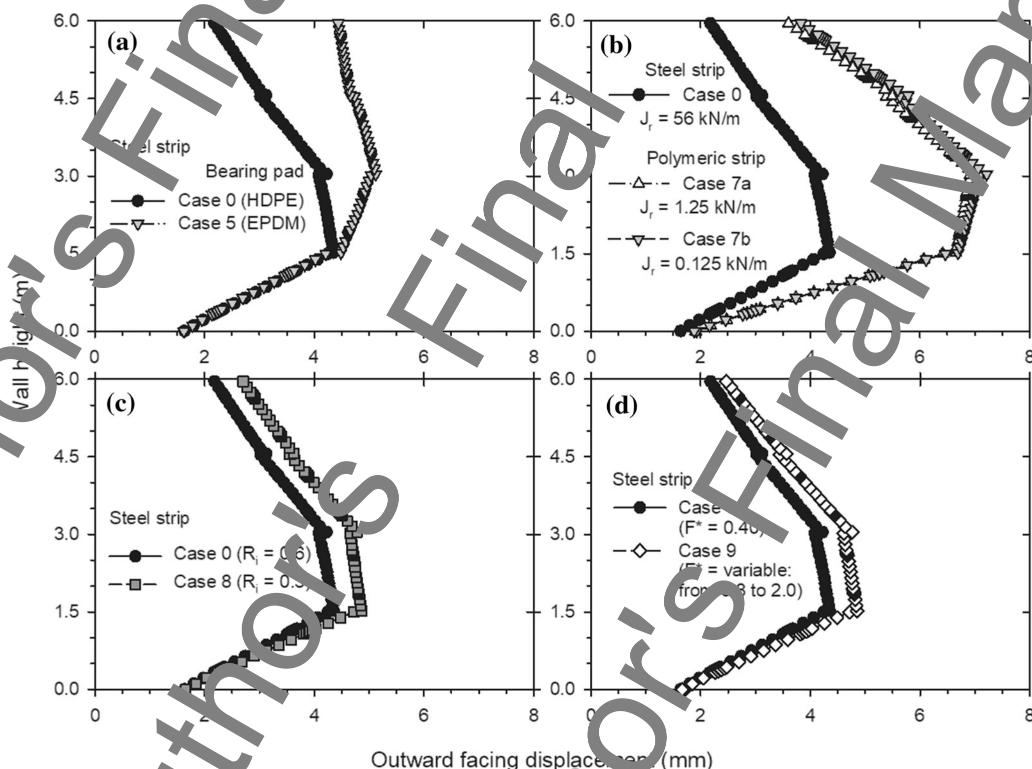

Fig. 6 Outward facing displacements with respect to original toe of wall at start of construction

adjustments to panel placement and alignment as construction proceeds.

The moving datum for monitoring points used to track wall facing deformation measurements in the field adds uncertainty to deformation analyses. Nevertheless, Miyata et al. [36] estimated out-of-vertical deformations of 10–190 mm (0.1–2.9% of wall height) from monitored polymeric strap walls of similar height to the wall in this study. The numerical models in the current study for the polymeric strap case gave 0.13% of the wall height and thus fall just inside the lower range of values available from field measurements.

The reinforced soil mass may also experience a competing backward rotation when seated on a compliant (compressible) foundation [19, 31]. This can be appreciated by the larger vertical displacements located within the reinforced soil zone in Fig. 5b compared to the front of the wall.

Figure 7 shows facing displacement profiles computed for different combinations of backfill and foundation modulus values. As the foundation modulus becomes less and all other parameter values remain unchanged, the horizontal deformation of the wall increases. For the weakest backfill and foundation soil combination (Case 1), the wall has the appearance of rotating backward.

Horizontal displacement profiles taken at the face and at selected distances from the face are presented in Fig. 8 for the base case (Case 0). The plots in this figure show that outward deflections are greatest at the face but decrease with distance from the face of the wall.

5.3 Reinforcement layer vertical settlements

Figure 9 shows vertical settlement profiles for selected layers using steel and polymeric strips. The datum for these plots is the elevation of the wall toe at start of wall construction. The settlements increase with distance from the facing and are greater for the more extensible polymeric strip material. The difference is a maximum of about 2 mm. For each case in each plot, the smallest settlements are close to the connections, which is consistent with hanging up of the soil over the reinforcement strips described earlier.

5.4 Reinforcement loads

Figure 10 shows reinforcement load distributions along the length of selected reinforcement layers. The four curves in each plot correspond to different combinations of reinforced soil and foundation soil modulus. Overall stiffness of the soil materials increases in the order of Case 1, 2, 3 and 4 as identified in Table 4. In general, the magnitude of reinforcement tensile loads increases in the reverse order when all other parameters remain unchanged. The exception occurs close to the connection with the facing particularly at the bottom-most layer (e.g. Layer 2 in Fig. 10). An explanation for this is the relatively low stiffness of the backfill soil located within 1 m of the facing.

An important observation from this figure is that the maximum tensile loads are greatest in the vicinity of the connections for the two stiffest reinforced soil conditions

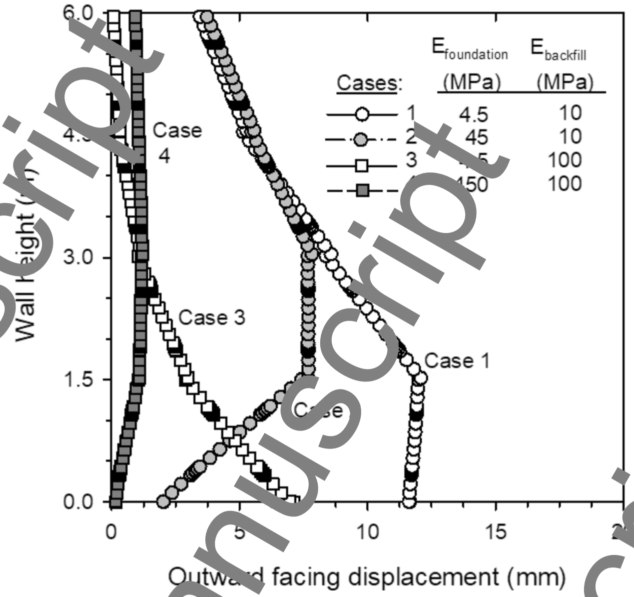

Fig. 7 Outward facing displacement profiles at end of construction (Cases 1, 2, 3 and 4)

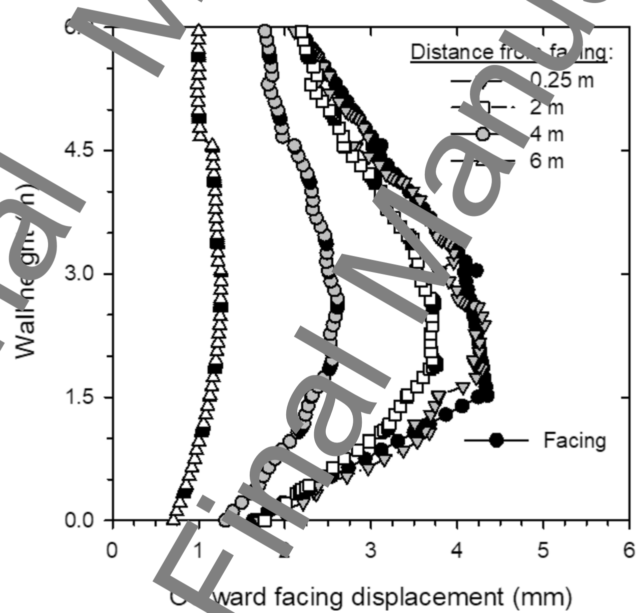

Fig. 8 Outward displacement profiles at face of wall to 6 m from facing at end of construction (Case 0)

while for the softer soil conditions the peak tensile load is located closer to the middle of reinforcement length. An implication for design is that the maximum tensile load should also be applied at the connections to be conservatively safe. This assumption is made in North American design codes for all MSE walls [1, 18], while in other codes (e.g. [11]; AFNOR [3]) the tensile load at the connections may be taken as some fraction of the computed maximum tensile load depending on the flexibility of the facing and the connection system.

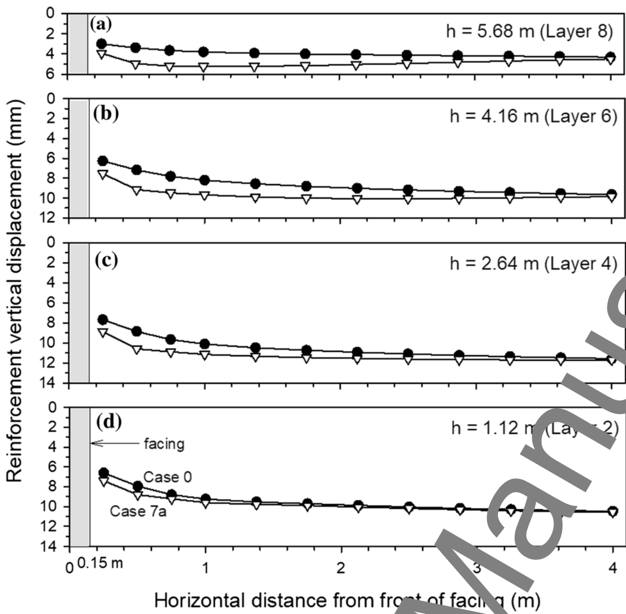

Fig. 9 Vertical settlement profiles for selected steel (Case 0) and polymeric strip reinforcement layers (Case 7a) at end of construction

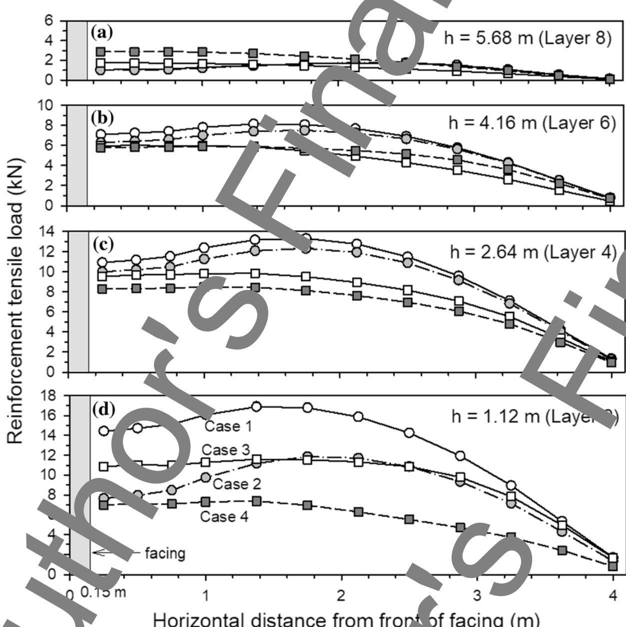

Fig. 10 Tensile reinforcement loads in selected reinforcement layers for Cases 1, 2, 3 and 4 showing influence of foundation and backfill soil modulus

In this study, numerical simulations were carried out to investigate the influence of bearing pad compressibility on wall performance. Results related to reinforcement tensile loads are shown in Fig. 11. Generally, maximum reinforcement loads are larger with the softer bearing pad arrangement (Case 5). Furthermore, for the softer bearing pad configuration the maximum reinforcement loads are at the connections. The larger tensile loads for the softer bearing pad configuration are consistent with the larger facing deformations for this wall compared to the same wall but with stiffer bearing pads (Fig. 6a). However, this relative performance difference may not occur for other combinations of soil modulus and reinforcement stiffness that were not examined in this study.

The influence of reinforcement stiffness on reinforcement loads is shown in Fig. 12. As may be expected, the reinforcement loads are much higher for the steel strip reinforced wall in comparison with the otherwise nominally identical two cases with stiffness values associated with more compliant PET strap walls. The stiffness of the two PET strap cases varies by a factor of 10, but the difference in loads varies by less than a factor of 2. The difference in peak reinforcement loads between steel and the stiffest PET strap case is a factor of 70, but the ratio of maximum loads is about 10. The nonlinear increase in reinforcement loads with reinforcement stiffness is in sympathy with the qualitative trend using the stiffness-based simplified stiffness method developed by Allen and Bathurst [5]. This method has been recently adopted by AASHTO [1] for the calculation of tensile loads for internal stability of MSE walls constructed with geosynthetic reinforcement materials.

Similar sensitivity analysis comparisons were carried out to isolate the influence of the strength and stiffness reduction factor on reinforced loads (Cases 8 and 9). These analyses showed no practical difference in reinforcement load magnitude and distribution and thus are not presented.

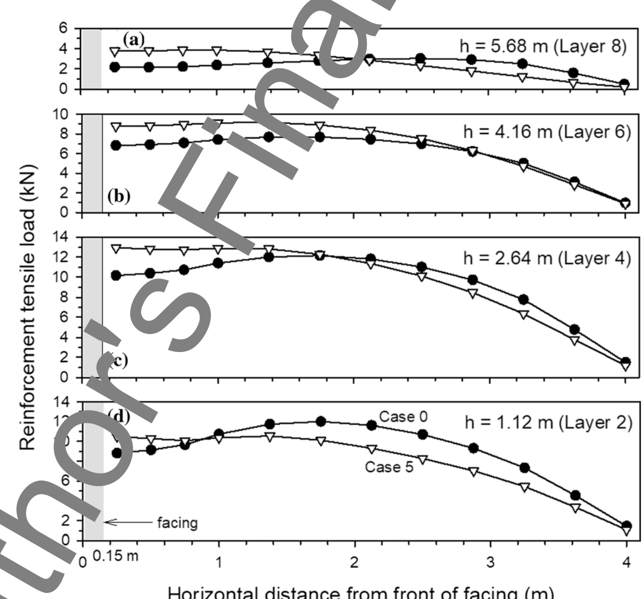

Fig. 11 Tensile reinforcement loads in selected reinforcement layers for Cases 0 and 5 (relatively stiff and soft bearing pads, respectively)

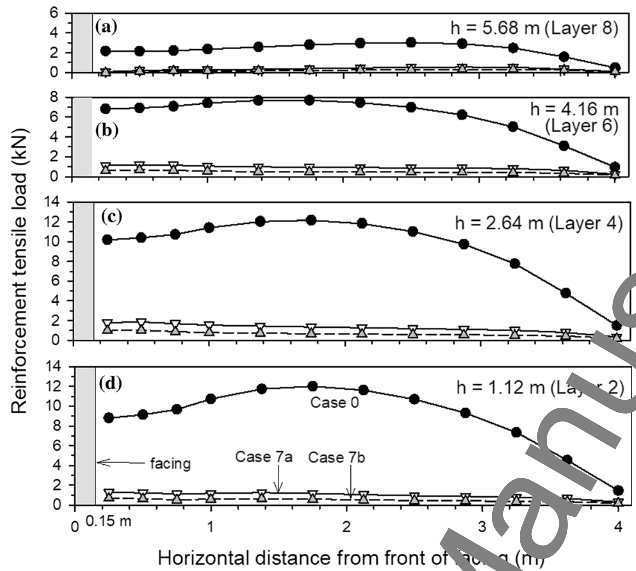

Fig. 12 Tensile reinforcement loads in selected reinforcement layers for Case 0 (relatively stiff steel reinforcement), and Cases 7a and 7b (relatively less stiff PET strap reinforcement)

6 Earth pressures

6.1 Vertical foundation pressures

Figure 13a shows the computed vertical foundation pressures and the vertical pressure exerted by the facing column on the footing for the base case (steel strip). Data with solid symbols are located directly at the midlocation of the wall below the centreline of the steel strips. The data points with open symbols reveal that the toe load pressures vary in the running length direction of the wall. This small three-dimensional effect cannot be detected using a 2D model. The distributions of foundation pressure corresponding to the same three locations were not practically detectable and for this reason are not plotted to avoid visual clutter. As discussed for the PWRI wall, the vertical toe pressure is greater than the pressure due to self-weight of the column panels (i.e. footing load factor > 1) due to down-drag on the back of the concrete panels and on the steel strips. The load factors are 2.82, 2.72 and 2.64 for points located at 0.125 m from the lateral boundaries, midpoint between lateral boundary and steel strip, and directly below the centreline of the steel strips, respectively.

Figure 13b shows the foundation pressures for the same case above but using the less stiff polymeric reinforcement (Case 7a). The foundation pressures are essentially unchanged, but the vertical toe pressures are less at the same locations along the running length of the wall. The load factors are now 2.58, 2.47 and 2.41 at the same locations as above. From a practical point of view, the differences between the two reinforcement cases with respect to the down-drag loads are not significant but they are detectable.

Figure 13c shows the results of calculations using other combinations of soil elastic modulus for the steel strip case. For the case of very stiff soil properties (Case 4), there is a relatively large reduction in vertical toe pressure compared to the other cases including Case 0. However, qualitative trends in the distribution of foundation pressures remain unchanged.

Finally, the computed load factors in Fig. 13a–c are typical for measured values reported in the literature for field walls [19] and most often fall within the recommended range of 2–3 for the design of the bearing pads for incremental concrete panel walls in the USA [25].

6.2 Vertical pressures at and in the vicinity of the reinforcement strips

A major motivation for the numerical simulations in this study was to investigate 3D behaviour which can be expected to be different from an equivalent 2D wall model. Figure 14 shows vertical pressure distributions computed at 0.25 m from the front of the facing panels. The plots in the figure show that:

1. Close to the facing, the vertical pressures at a height of 2.5 cm above the strips are greater than the soil self-weight at this location. At 15 cm above the strips, vertical pressures are attenuated to about one-half those at 2.5 cm above the strips. The explanation for this behaviour is that the block of soil behind the wall facing wants to move down with respect to the wall face as the facing moves outward and the soil compresses. The reinforcement strip impedes this movement, and the soil hangs up on the strip. The soil located between the strips then imparts down-drag forces on the soil column above the strip. This results in greater normal stress on top of the strip than soil at the same elevation and located on either side of the strip.
2. The vertical pressures directly below the strips decrease with decreasing distance from the strip and are less than the constant pressure recorded beyond about 20 cm of the strip centre at the same elevation. It should be noted that a small amount of soil cohesion (c = 1 kPa in Table 1) was used in the model to avoid numerical instability at the free boundaries. This resulted in very small negative vertical stresses directly below the reinforcement strips as shown in Fig. 14. From a practical point of view, these stresses should be assumed as zero.
3. The lateral distance over which vertical pressures close to the back of the facing panel are modified by the steel

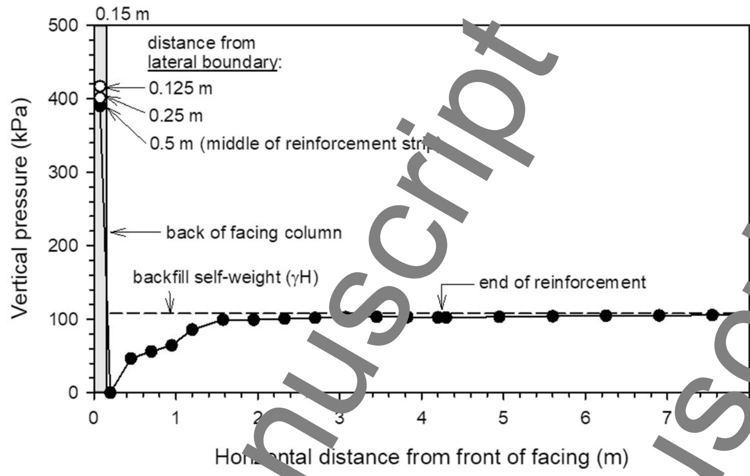

(a) Base Case 0 (steel reinforcement)

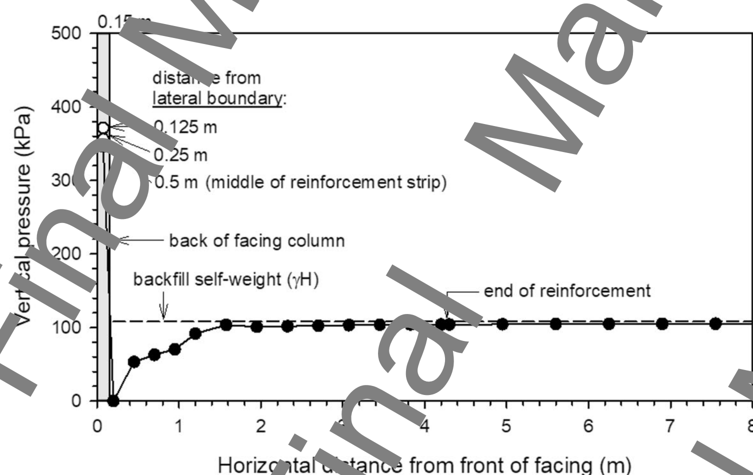

(b) Case 7a (polymeric strip)

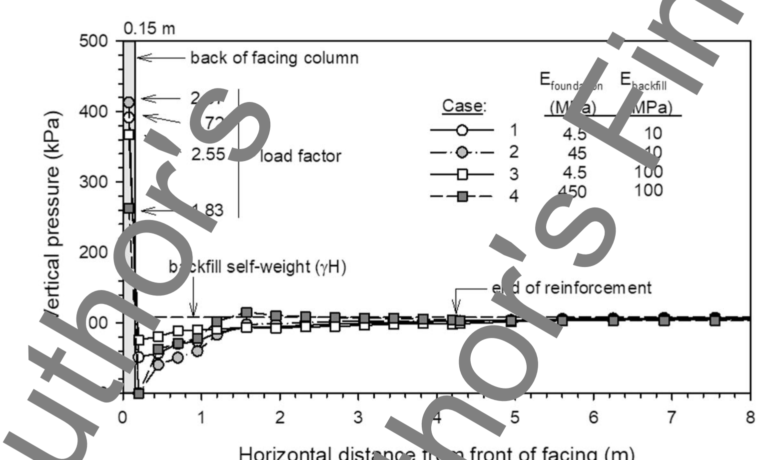

(c) Cases 1, 2, 3 and 4. Pressures directly below the centreline of the steel strip reinforcement strips

Fig. 13 Vertical foundation pressures at end of construction

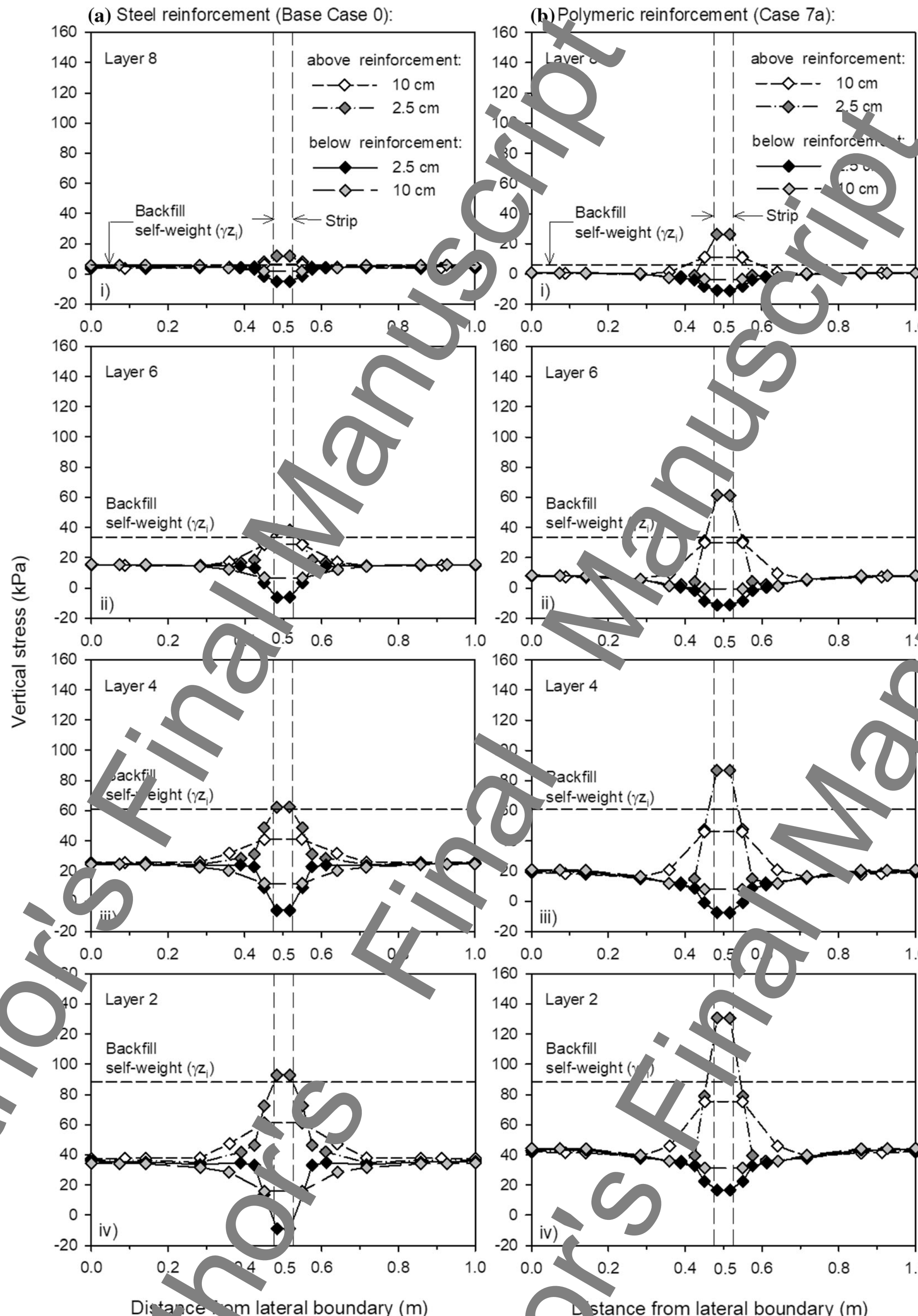

Fig. 14 Vertical pressure distributions at and in the vicinity of the reinforcement strips at 0.25 m from the back of the facing for **a** steel reinforcement base Case 0 and **b** polymeric reinforcement (Case 7a)

strip inclusion is about 5B where $B = 0.05$ m is the strip width (Fig. 14a).

4. The magnitude of increased vertical pressure acting on the strips increases with depth of the reinforcement strip below the top of the wall.

Author's Final Manuscript

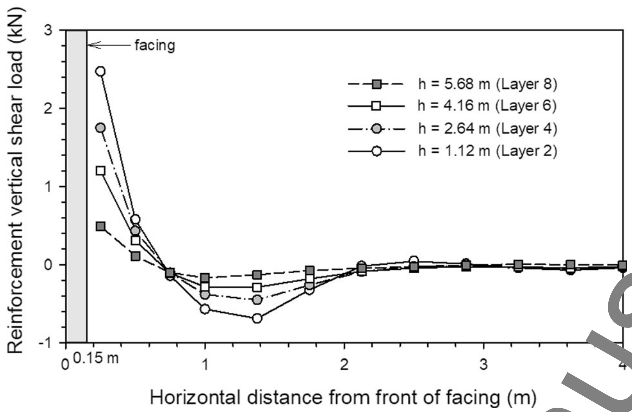

Fig. 15 Vertical shear load along length of steel strip reinforcement layers (Case 0)

5. The maximum vertical pressure acting on Layer 2 close to the back of the facing is about a factor of 2 and 3 greater than the pressure beyond the edges of the steel and polymeric reinforcement layers, respectively.
6. Qualitative features are the same for steel and polymeric cases. However, Layer 2 of the stiffer steel strip wall has slightly lower maximum vertical pressure above the strip than the matching polymeric strap. For the topmost Layer 8, the polymeric strap carries greater vertical pressure as well. The larger vertical pressure is consistent with the greater settlement computed for the polymer strip reinforced wall compared to the steel reinforcement case (Fig. 9).

The increase in vertical pressure acting over the strips close to the back of the facing column is consistent with the hanging up of the soil on the reinforcement strips that leads to the foundation pressure attenuation immediately behind the facing that was described earlier. A practical implication of the observations made above is that the over-pressure acting on the strips can be used to check against shear failure of rigid connectors between the reinforcement strips and panels. For example, Fig. 15 shows a plot of vertical shear load through the steel strips for the base case example with a fixed connection. The maximum shear loads are at the connections as expected, but the loading is well below the connection shear capacity. Deformations of the steel strips at the connections due to connection type can also be investigated (e.g. rigidly fixed connector or a connector with rotational degree of freedom).

Figure S3 in the Supplemental Material for this paper shows similar plots to Fig. 14 taken at 2.0 m from the front of the facing. At this location, the pressure distributions are almost flat, indicating that the interference of the reinforcement strips on vertical pressures above and below the strip elevations has largely dissipated at this location.

6.3 Lateral earth pressures

Figure 16a shows the horizontal earth pressures acting at the back of the facing in the reinforcement direction and in the wall direction at the centreline location of the steel reinforcement strips. Sharp jumps can be observed in the pressure profiles against the facing (open symbols). These pressures are larger just above the top of the reinforcement strip compared to just below. This behaviour is consistent with the larger and smaller vertical pressures at the same location in Fig. 14. The corresponding profile (Fig. 16b) taken through the same height of the wall but at the mid-point between the strip centreline and the lateral boundary can be seen to be smoother. This is because the disturbance to the earth pressure distribution due to the reinforcement inclusions is attenuated with distance from the reinforcement.

The same qualitative trends can be seen for the more extensible polymeric strip reinforcement in Fig. 16c, d. However, the pressures against the wall are lower than for the less extensible steel reinforcement strip cases. In fact, the pressures at locations between and beyond the immediate influence of the reinforcement layers are typically in the vicinity of K_a values or less. For the steel strip case, the pressures in those same locations are most often greater than the K_a value and often in the vicinity of K_o values. The lower pressures for the polymeric strip case compared to the relatively inextensible steel strip case are in sympathy with classical notions of earth pressure theory that predict lower earth pressures with greater lateral deformations.

Also shown in the plots of Fig. 16 are lateral pressures (solid grey symbols) at the same location but in the orthogonal direction (i.e. in the running direction of the wall face—direction x in Fig. 1). For the steel strip cases, the orthogonal pressures are most often similar in magnitude to those acting against the facing. However, for the matching case with more extensible polymeric strips, the orthogonal pressures are most often greater and by a relatively large amount at some locations.

In conventional analytical design approaches to compute earth pressures acting against the facing, the out-of-plane soil stresses cannot be considered. However, frictional soils are stress-level dependent and ignoring the larger lateral stresses computed in the out-of-plane direction in 3D numerical models will underestimate the mean confining stress in the soil, thus making the soil appear weaker and less stiff. The recommendation to include the out-of-plane stress (σ_x) in the calculation of the bulk modulus in non-linear constitutive models for frictional soils has been made by Huang et al. [29] and Yu et al. [51, 52] to improve the accuracy of numerical models for reinforced soil walls with continuous sheet reinforcement.

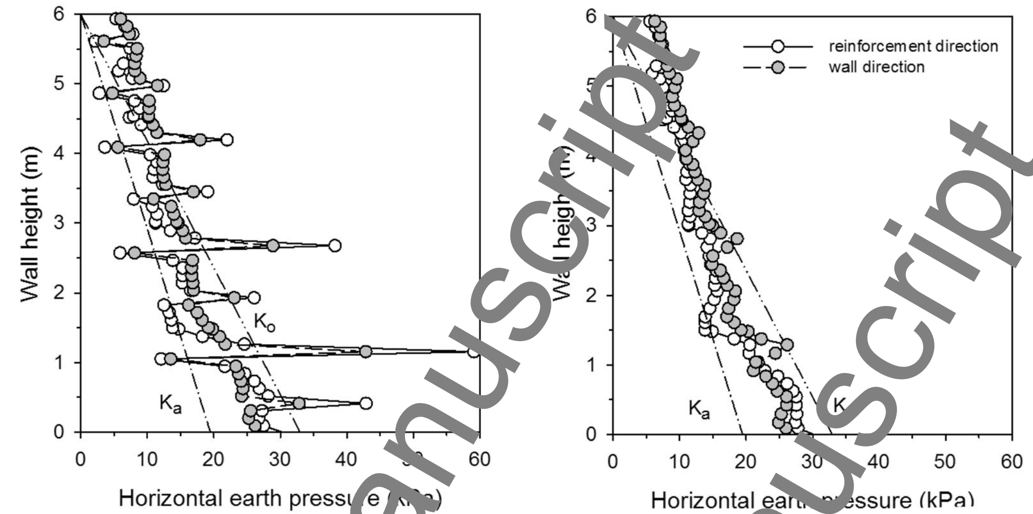

(a) at centreline of reinforcement layer (steel strip – Case 0)

(b) at midpoint between reinforcement layer and lateral boundary (steel strip – Case 0)

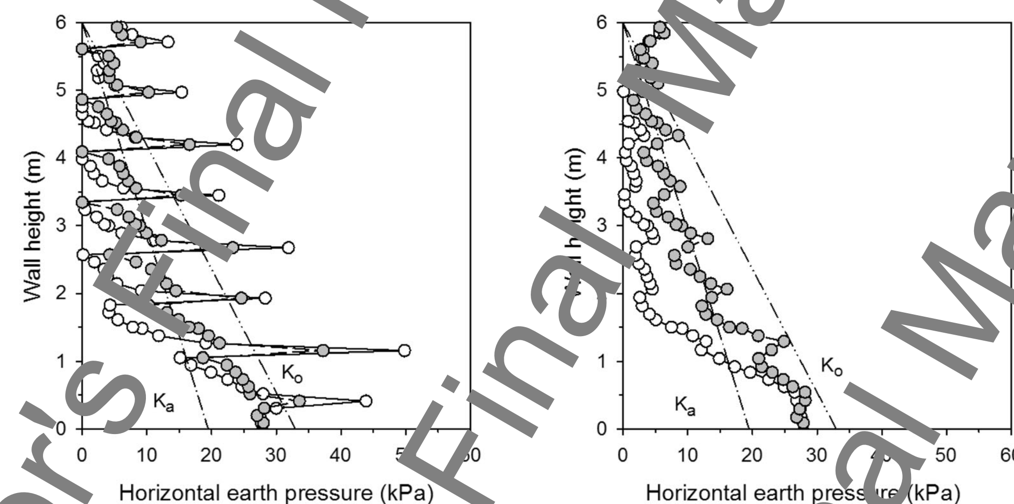

(c) at centreline of reinforcement layer (polymeric strip – Case 7a)

(d) at midpoint between reinforcement layer and lateral boundary (polymeric strip – Case 7b)

Fig. 16 Lateral earth pressures at back of facing in reinforcement direction and in wall direction. *Note*: Pressures computed at 0.25 m from back of facing

7 Conclusions

This paper reports the first attempt to carry out 3D numerical modelling of a tall (6-m-high) vertical slice of a MSE wall constructed with steel strip reinforcement since the work of Ho and Smith [28]. The 3D model was used to predict the influence of reinforcement type on wall performance using the examples of relatively inextensible (steel strip) and relatively extensible (polymeric strip) materials that are common components in MSE walls constructed today.

The paper demonstrates that the 3D model does not have practical advantage over simple 2D models for walls with simple reinforcement arrangements and no surface loading when comparisons are limited to tensile reinforcement loads and careful attention is paid to choice of parameters for the soil, strip reinforcement and the facing parameters. However, the advantage of the general 3D model approach is that the influence of the discrete reinforcement strips on numerical predictions of the magnitude and distribution of pressures acting on the wall facing and on the steel strips is detectable. This is not possible using 2D continuous reinforcement sheet approximations to rows of discrete reinforcement strips as is the approach used most often today. The ability to model the MSE wall components in 3D holds promise to better predict the tensile loads in the reinforcement strips/straps (particularly when reinforcement strips are placed at variable spacing in a layer), evaluate stresses in the facing panels (Figure S4) and compute shear loads at the connections. These advantages can assist to avoid over-stressing at these locations and to optimise wall design. However, the connection details in the numerical models used in this study are purposely kept simple. Connection performance predictions can be expected to change as model details at the location of the connections are improved.

A disadvantage of the modelling approach in this paper is that computational demands are large, at least for typical high-end desktop computers that are currently available. However, this is expected to be less of a problem in the future. Hence, this study holds promise to provide guidance to designers for taller and more complex strip reinforced MSE walls as 3D numerical modelling software suitable for MSE wall structures improves and computational power increases.

Acknowledgements The authors wish to acknowledge the support of the International Center for Numerical Methods in Engineering (CIMNE) and the funding received from the Spanish Ministry of Economy and Competitiveness through the "Severo Ochoa Programme for Centres of Excellence in R&D" (CEX2018-000797-S), and the Natural Sciences and Engineering Research Council of Canada (NSERC) (Grant Number: 94344-2013).

References

1. AASHTO (2020) AASHTO LRFD Bridge design specifications, 9th Ed. American Association of State Highway and Transportation Officials. Washington, DC., USA
2. Abdelouhab A, Dias D, Freitag N (2011) Numerical analysis of the behaviour of mechanically stabilized earth walls reinforced with different types of strips. Geotext Geomembr 29(2):116–129
3. AFNOR (Association Française de Normalisation) (2009) Geotechnical design—Retaining structures—Reinforced and soil nailing structures. NFP 94-270. Paris: AFNOR
4. Allen TM, Bathurst RJ (2014) Performance of a 11 m high block-faced geogrid wall designed using the K-stiffness Method. Can Geotech J 51(1):16–29
5. Allen TM, Bathurst RJ (2015) An improved simplified method for prediction of loads in reinforced soil walls. ASCE J Geotechn Geoenviron Eng 141(11):04015049
6. Allen TM, Bathurst RJ (2018) Application of the Simplified Stiffness Method to design of reinforced soil walls. ASCE J Geotechn Geoenviron Eng 144(5):04018024
7. Allen TM, Bathurst RJ (2019) Geosynthetic reinforcement stiffness characterization for MSE wall design. Geosynth Int 26(6):592–610
8. Bathurst RJ, Miyata Y, Allen TM (2020) Deterministic and probabilistic assessment of margins of safety for internal stability of as-built PET strap reinforced soil walls. Geotex Geomembr (availabe online). https://doi.org/10.1016/j.geotexmem.2020.06.001
9. Bourgeois E, Soyez L, Le Kouby A (2011) Experimental and numerical study of the behavior of a reinforced-earth wall subjected to a local load. Comput Geotech 38(4):515–525
10. Bourgeois E, Le Kouby A, Soyez L (2012) Influence of the strip–backfill interaction model in the analysis of the behavior of a mechanically stabilized earth wall. Soils Found 52(3):550–561
11. BSI (2010) BS8006-1:2010 + A1:2016 code of practice for strengthened/reinforced soil and other fills. BSI, Milton Keynes
12. Cai Z, Bathurst RJ (1995) Seismic response analysis of geosynthetic reinforced soil segmental retaining walls by finite element method. Comput Geotech 17(4):523–546
13. Capilleri PP, Ferraiolo F, Motta E, Scotto M, Todaro M (2019) Static and dynamic analysis of two mechanically stabilized earth walls. Geosynth Int 26(1):26–41
14. CODE_BRIGHT User's Guide (2016) Department of Civil and Environmental Engineering, Barcelona School of Civil Engineering, Universitat Politècnica de Catalunya (UPC) and International Center for Numerical Methods in Engineering (CIMNE). https://deca.upc.edu/ca/el-departament/seccions/etcg/recerca/projectes/code_bright https://www.gidhome.com/gid-plus/modules/modules-research/27/codebright/
15. Chida S, Nakagaki M (1979) Test and experiment on a full-scale model of reinforced earth wall. In Proceedings of international conference on soil reinforcement, Paris, vol II, pp 533–538
16. Choufani C, Wu P, Gagnon G, Macintosh M (2011) A precast faced mechanical stabilized earth solution for a 30 metre high mining crusher wall with various technical and site challenges. In Proceedings of 2011 Pan-Am Canadian geotechnical conference (CD-ROM), Canadian Geotechnical Society, Richmond, BC, Canada, 625
17. Cristelo N, Félix C, Lopes ML, Dias M (2016) Monitoring and numerical modelling of an instrumented mechanically stabilised earth wall. Geosynth Int 23(1):48–61
18. CSA (2019) Canadian Standards Association (CSA). Canadian Highway Bridge Design Code. CAN/CSA-S6-19, Mississauga, Ontario, Canada
19. Damians IP, Bathurst RJ, Josa A, Lloret A, Albuquerque PJR (2013) Vertical facing loads in steel reinforced soil walls. ASCE J Geotech Geoenviron Eng 139(9):1419–1432
20. Damians IP, Bathurst RJ, Josa A, Lloret A (2014) Numerical study of the influence of foundation compressibility and reinforcement stiffness on the behavior of reinforced soil walls. Int J Geotech Eng 8(3):247–259
21. Damians IP, Bathurst RJ, Josa A, Lloret A (2015) Numerical analysis of an instrumented steel reinforced soil wall. ASCE Int J Geomech 15(1):04014037
22. Damians IP, Yu Y, Lloret A, Bathurst RJ, Josa A (2015b) Equivalent interface properties to model soil-facing interactions with zero-thickness and continuum element methodologies. In: XV Pan-American conference on soil mechanics and geotechnical engineering (XV PCSMGE), from fundamentals to applications in geotechnics. Buenos Aires, Argentina. 15th–18th November 2015, pp 1065–1072
23. Damians IP, Bathurst RJ, Josa A, Lloret A (2016) Vertical facing panel-joint gap analysis for steel-reinforced soil walls. ASCE Int J Geomech 16(4):04015103
24. Fan CC (2006) Three-dimensional behaviour of a reinforced earth-retaining structure within a valley. Comput Geotech 33(2):69–85
25. FHWA (2009) Design of mechanically stabilized earth walls and reinforced slopes. In: Berg RR, Christopher BR, Samtani NC (eds) No. FHWA-NHI-10-024 Vol I and NHI-10-025 Vol II, Federal Highway Administration, Washington, DC., USA

26. Hatami K, Bathurst RJ (2006) Numerical model for reinforced soil segmental walls under surcharge loading. ASCE J Geotech Geoenviron Eng 132(6):673–684
27. Hatami K, Bathurst RJ (2005) Development and verification of a numerical model for the analysis of geosynthetic reinforced soil segmental walls under working stress conditions. Can Geotech J 42(4):1066–1085
28. Ho DKH, Smith IM (1991) Modelling of reinforced soil wall: construction by a 3-D finite element method. Paper P4/6. In: McGown A, Yeo K, Andrawes KZ (eds) Performance of reinforced soil structures. Thomas Telford Publishing, London, pp 335–340
29. Huang B, Bathurst RJ, Hatami K (2009) Numerical study of reinforced soil segmental walls using three different constitutive soil models. ASCE J Geotech Geoenviron Eng 135(10):1486–1498
30. Itasca (2011) FLAC: Fast Lagrangian Analysis of Continua. Version 7.0. Itasca Consulting Group, Inc., Minneapolis, MN, USA
31. Jones CJFP, Edwards LW (1980) Reinforced earth structures situated on soft foundations. Geotechnique 30(2):207–213
32. Karpurapu RG, Bathurst RJ (1995) Behaviour of geosynthetic reinforced soil retaining walls using the finite element method. Comput Geotech 17(3):279–299
33. Kulhawy FH, Mayne PW (1990) Manual on estimating soil properties for foundation design. Report EL-6800, Electric Power Research Institute (EPRI). Palo Alto, California, p 306
34. Ling HI, Leshchinsky D (2003) Finite element parametric study of the behavior of segmental block reinforced-soil retaining walls. Geosynth Int 10(3):77–94
35. Lo SCR (1998) Pull-out resistance of polyester straps at low overburden stress. Geosynth Int 5(4):361–382
36. Miyata Y, Bathurst RJ, Allen TM (2018) Evaluation of tensile load model accuracy for PET strap MSE walls. Geosynth Int 25(6):656–671
37. Miyata Y, Bathurst RJ, Allen TM (2019) Calibration of PET strap pullout models using a statistical approach. Geosynth Int 26(4):413–427
38. Naylor DJ, Richards H (1978) Slipping strip analysis of reinforced earth. Int J Numer Anal Meth Geomech 2(4):343–366
39. Olivella S, Gens A, Carrera J, Alonso EE (1996) Numerical formulation for a simulator (CODE_BRIGHT) for the coupled analysis of saline media. Eng Comput 13(7):87–112
40. PLAXIS (2008) Reference Manual, 2D: Version 9.02. PLAXIS B.V., Delft University of Technology, Netherlands (http://www.plaxis.nl/)
41. PLAXIS (2012) Material Models Manual. PLAXIS B.V., Delft University of Technology, Netherlands
42. Rowe RK, Ho S (1997) Continuous panel reinforced soil walls on rigid foundations. ASCE J Geotechn Geoenviron Eng 123(10):912–920
43. Rowe RK, Skinner GD (2001) Numerical analysis of geosynthetic reinforced retaining wall constructed on a layered soil foundation. Geotex Geomembr 19(7):387–412
44. Runser DJ (1999) 17 m tall reinforced earth retaining wall. M.S. thesis, School of Civil Engineering, Purdue University, West Lafayette, Indiana, USA
45. Runser DJ, Fox PJ, Bourdeau PL (2001) Field performance of a 17 m-high reinforced soil retaining wall. Geosynth Int 8(5):367–391
46. Siemens GA, Bathurst RJ, Miyata Y (2018) Numerical simulation and parametric analysis of multi-anchor walls using the finite element method. Transp Geotech 15:57–69
47. Yoo C, Kim SB (2008) Performance of a two-tier geosynthetic reinforced segmental retaining wall under a surcharge load: full-scale load test and 3D finite element analysis. Geotext Geomembr 26(6):460–472
48. Yoo C, Jang YS, Park IJ (2011) Internal stability of geosynthetic-reinforced soil walls in tiered configuration. Geosynth Int 18(2):74–83
49. Yu Y, Bathurst RJ, Miyata Y (2015) Numerical analysis of a mechanically stabilized earth wall reinforced with steel strips. Soils Found 55(3):536–547
50. Yu Y, Damians IP, Bathurst RJ (2015) Influence of choice of FLAC and PLAXIS interface models on reinforced soil-structure interactions. Comput Geotech 65:164–174
51. Yu Y, Bathurst RJ, Allen TM, Nelson R (2016) Physical and numerical modelling of a geogrid reinforced incremental concrete panel retaining wall. Can Geotech J 53(12):1883–1901
52. Yu Y, Bathurst RJ, Allen TM (2016) Numerical modelling of the SR-18 geogrid reinforced modular block retaining walls. ASCE J Geotech Geoenviron Eng 142(5):04016003
53. Zevgolis IE (2018) A finite element investigation on displacements of reinforced soil walls under the effect of typical traffic loads. Transp Infrastruct Geotechnol 5(3):231–249

Publisher's Note Springer Nature remains neutral with regard to jurisdictional claims in published maps and institutional affiliations.

SUPPLEMENTAL MATERIAL

3D MODELLING OF STRIP REINFORCED MSE WALLS

https://doi.org/10.1007/s11440-020-01057-w

I.P. Damians
R.J. Bathurst
S. Olivella
A. Lloret
A. Josa

a) Step 1: foundation turned on

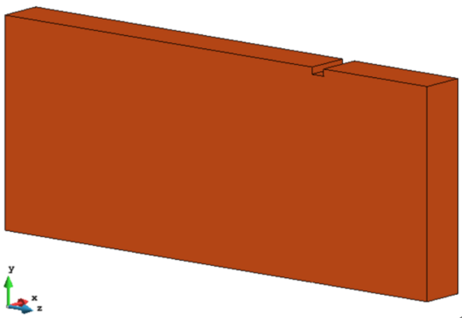

b) Step 2: leveling pad and panel 1 placed with braced support

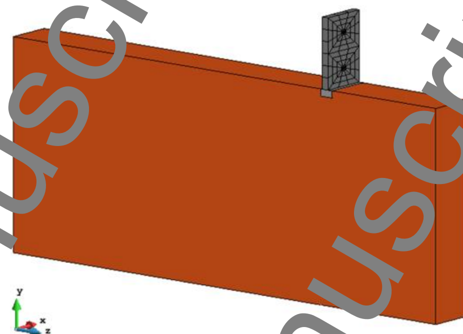

c) Step 3: 0.75 m of soil

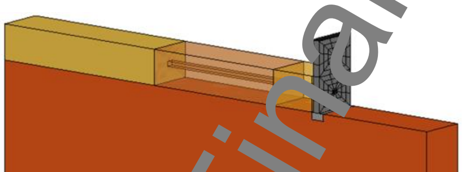

d) Step 4: bearing pad and panel 2 placed with braced support

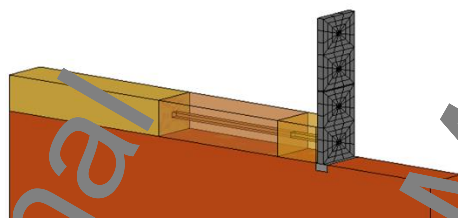

e) Step 5: 1.5 m of soil

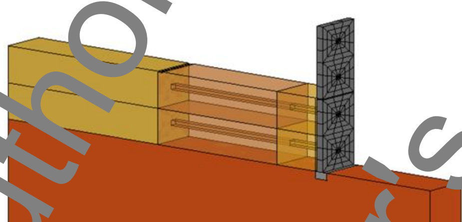

f) Step 6: 2.25 m of soil

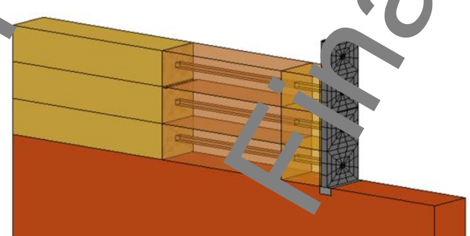

g) Step 7: bearing pad and panel 3 placed with braced support

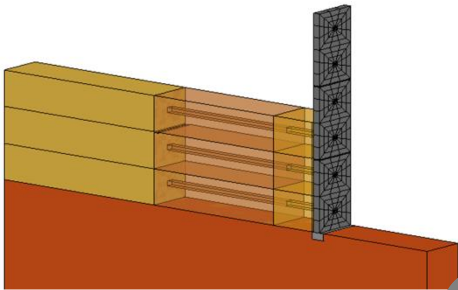

h) Step 8: 3.0 m of soil, braced support for panel 1 removed

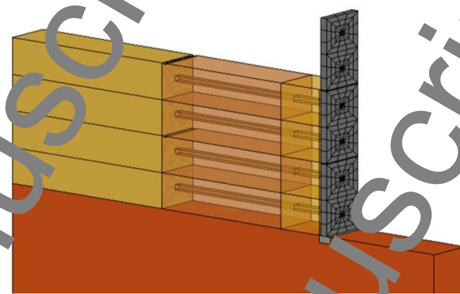

i) Step 9: 3.75 m of soil

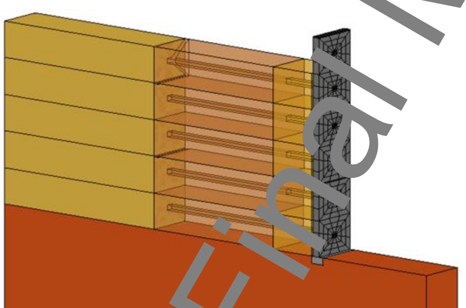

j) Step 10: bearing pad and panel 3 placed with braced support

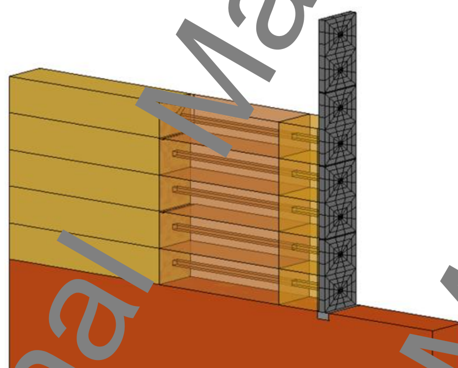

k) Step 11: 4.5 m of soil, and then braced support for panel 2 removed

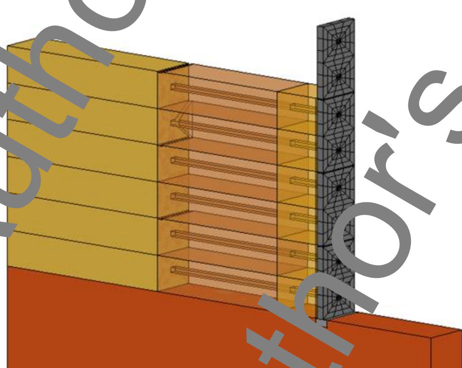

l) Step 12: 5.25 m of soil

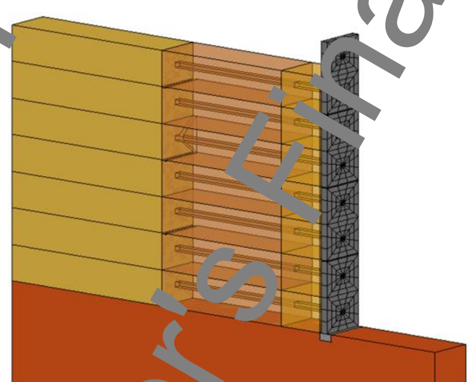

m) Step 13: 6.0 m of soil in placed all braced supports removed

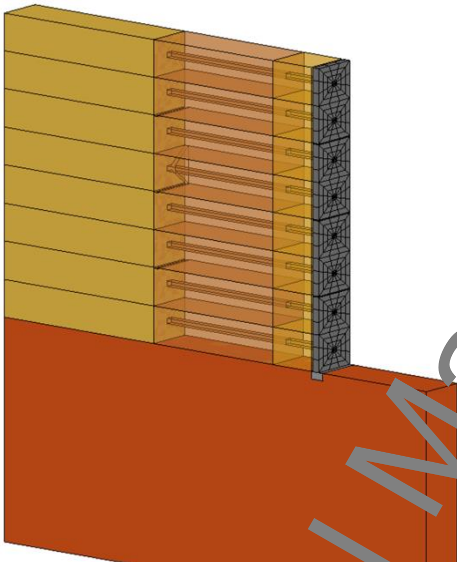

Figure S1: Illustration of staged construction of 6 m-high steel strip reinforced soil wall

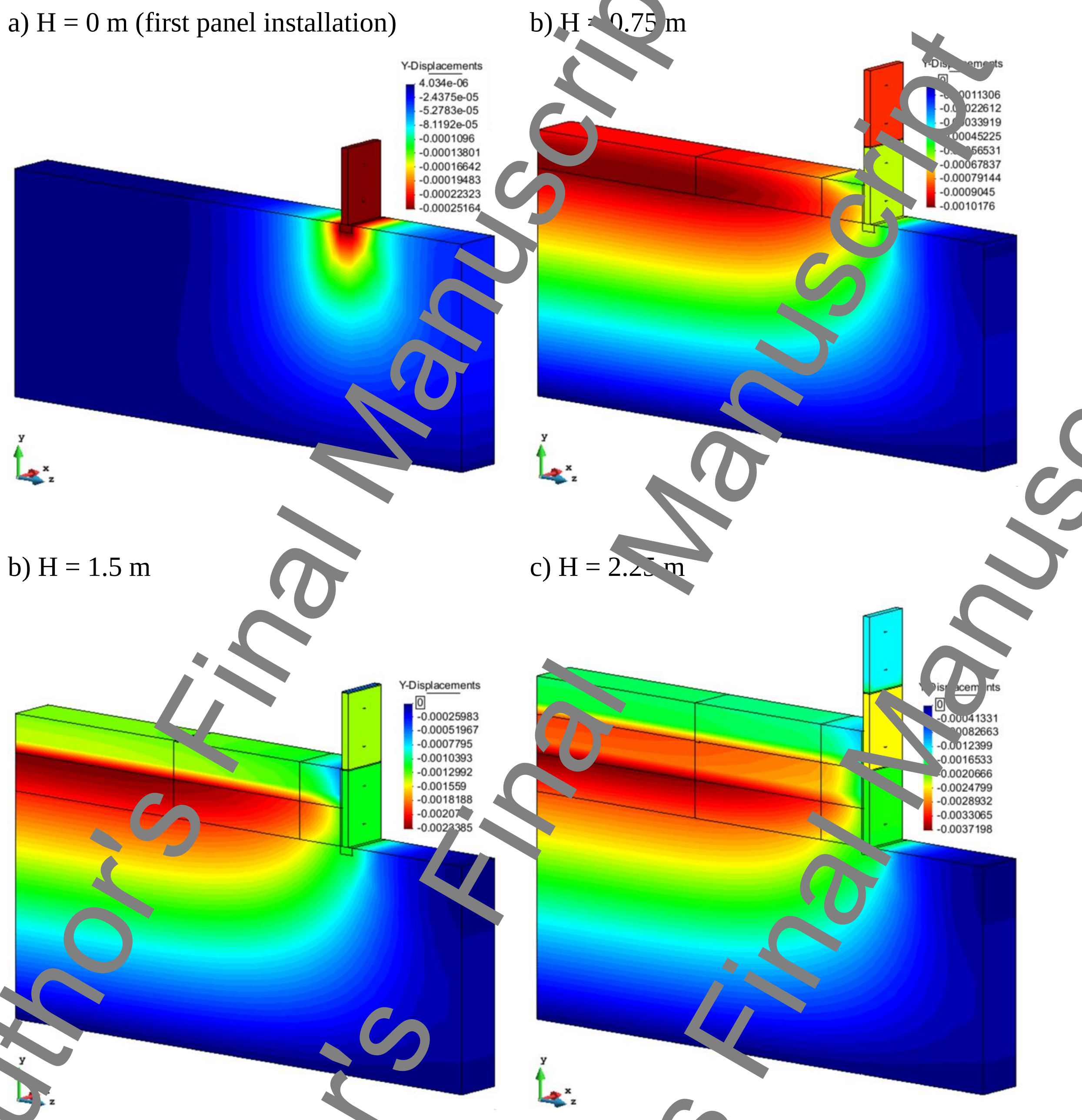
a) H = 0 m (first panel installation)
Y-Displacements
4.034e-06
-2.4375e-05
-5.2783e-05
-8.1192e-05
-0.0001096
-0.00013801
-0.00016642
-0.00019483
-0.00022323
-0.00025164
b) H = 0.75 m
-0.0010176
b) H = 1.5 m
Y-Displacements
0
-0.00025983
-0.00051967
-0.0007795
-0.0010393
-0.0012992
-0.001559
-0.0018188
c) H = 2.25 m
-0.0012399
-0.0016533
-0.0020666
-0.0024799
-0.0028932
-0.0033065
-0.0037198

d) H = 3.0 m

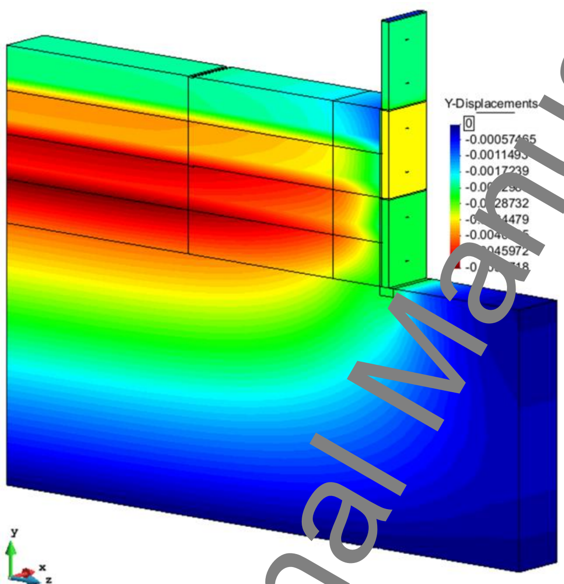

e) H = 3.75 m

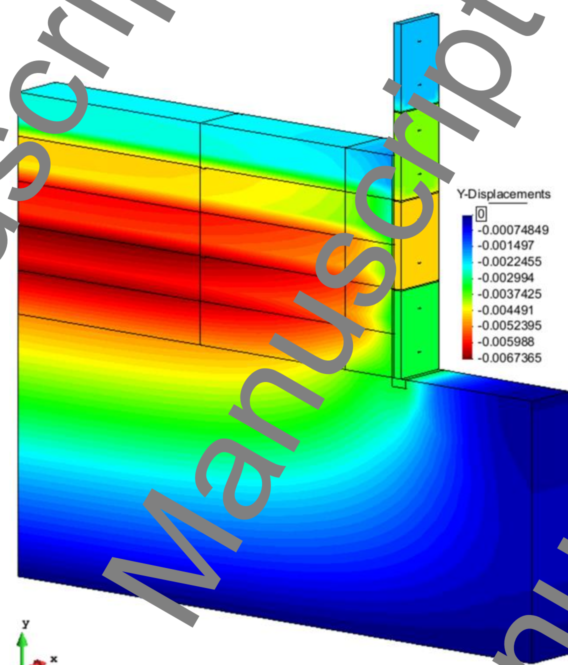

f) H = 4.5 m

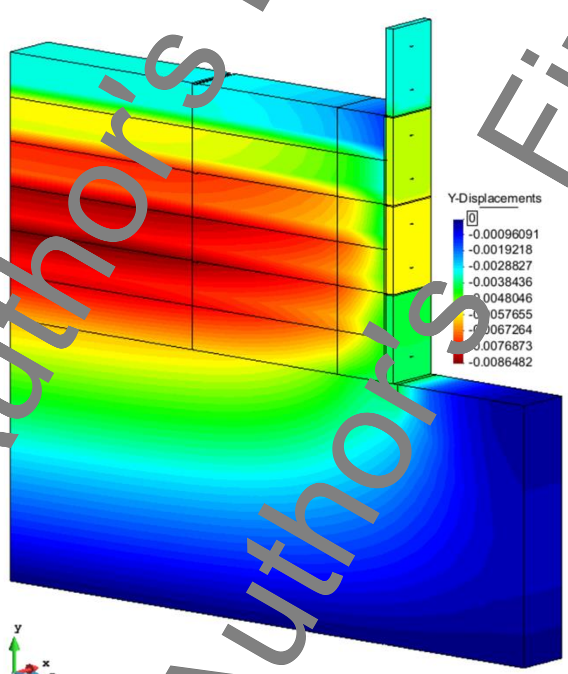

g) H = 5.25 m

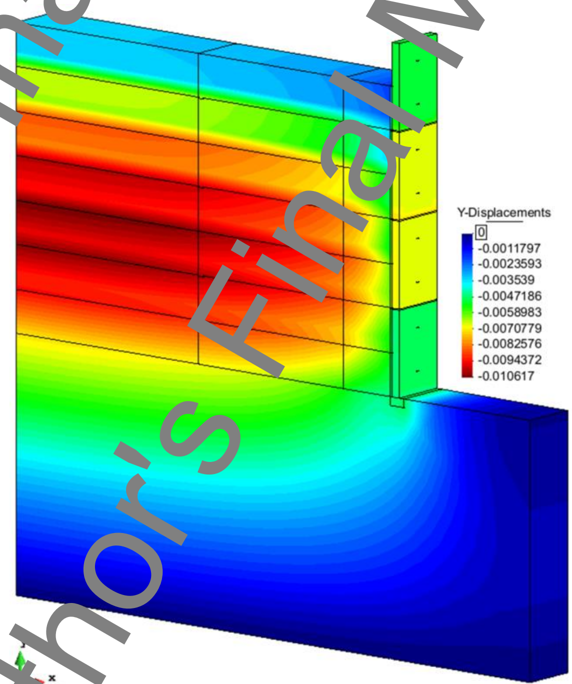

h) H = 6 m

i) H = 6 m (horizontal displacements)

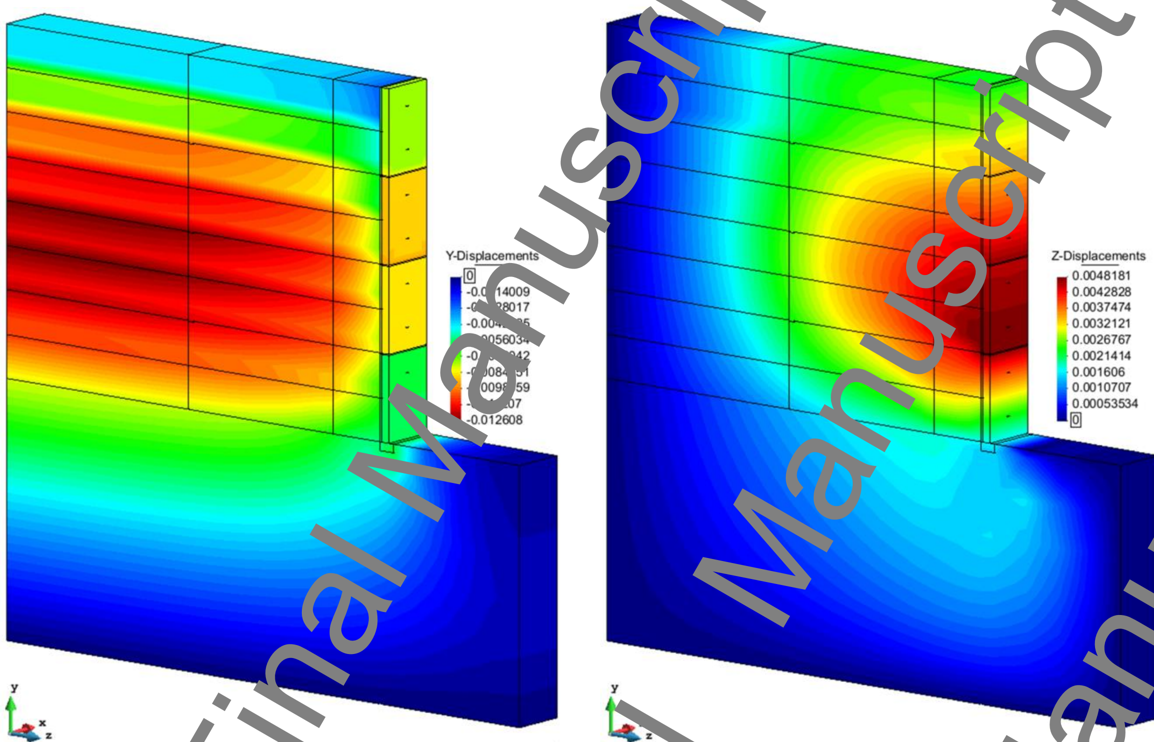

Figure S2. Vertical displacements at different construction stages (a-h) and horizontal wall displacements at end of construction H = 6 m (i) (units: m) (Case 0 – steel strip wall)

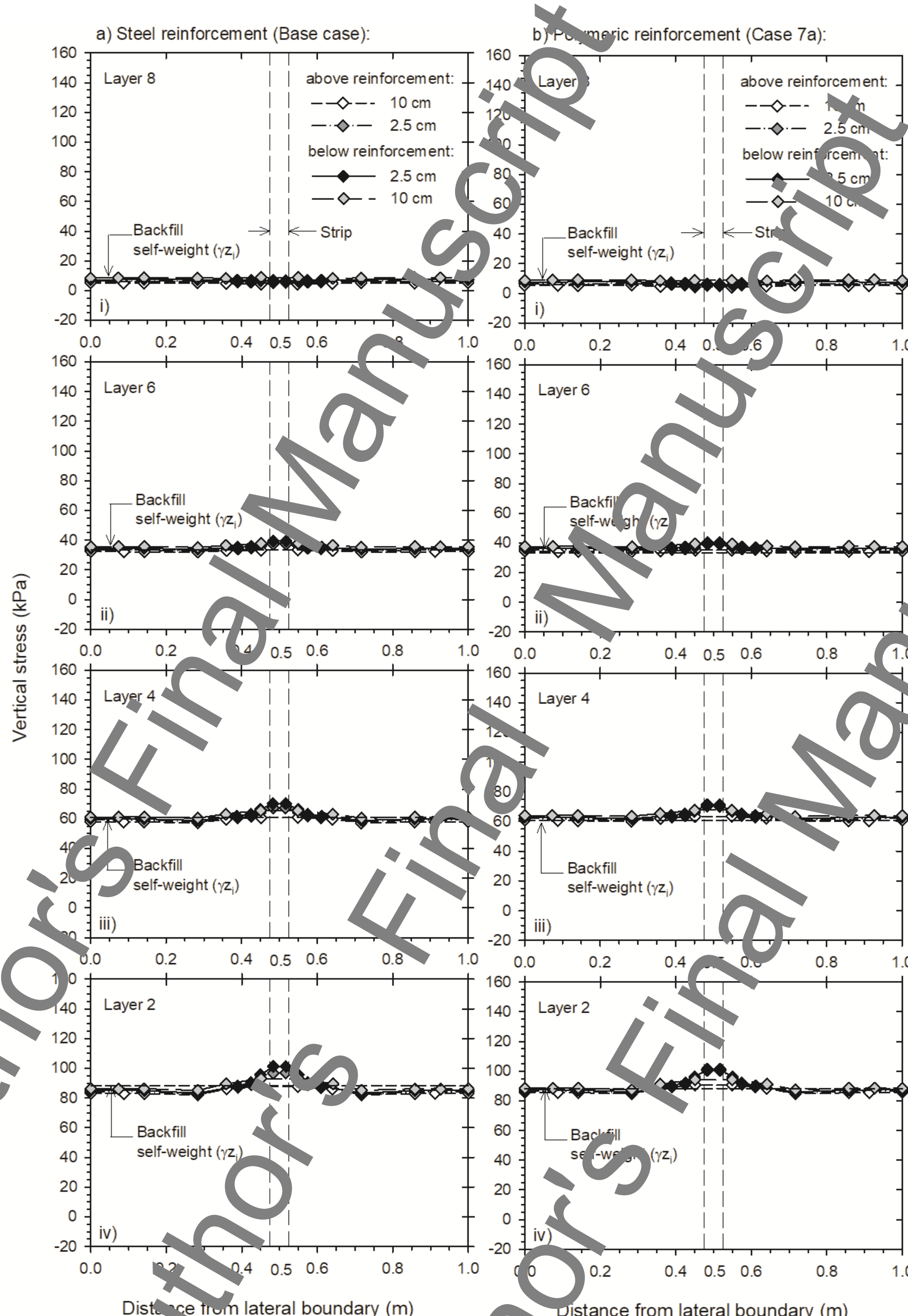

Figure S3. Vertical pressure distributions at and in the vicinity of the reinforcement strips at 2.0 m from front of the facing for: a) steel reinforcement base case (Case 0), and b) polymeric reinforcement (Case 7a).

a) vertical stresses (MPa)

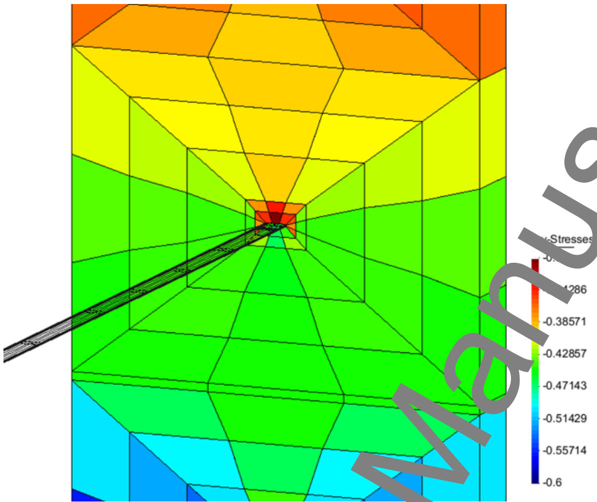

b) horizontal stresses (MPa) in reinforcement direction

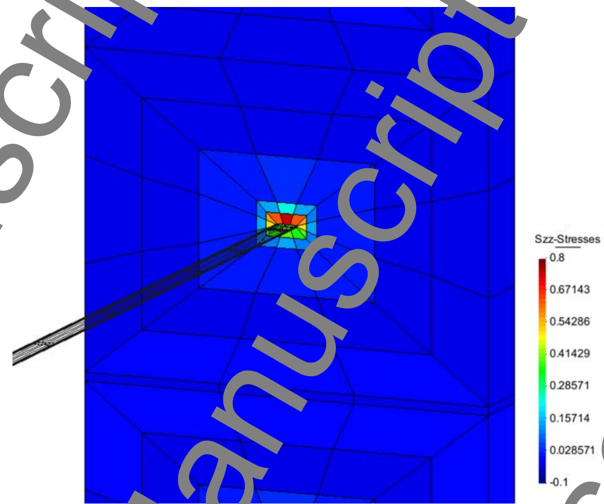

c) horizontal stresses (MPa) in wall face direction

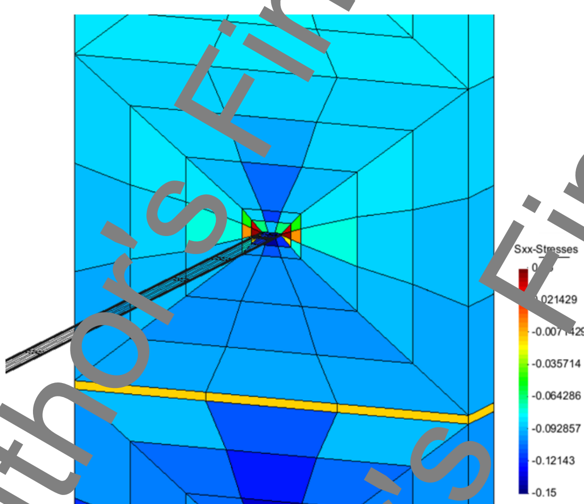

d) vertical strains (-) in panel and first horizontal panel joint

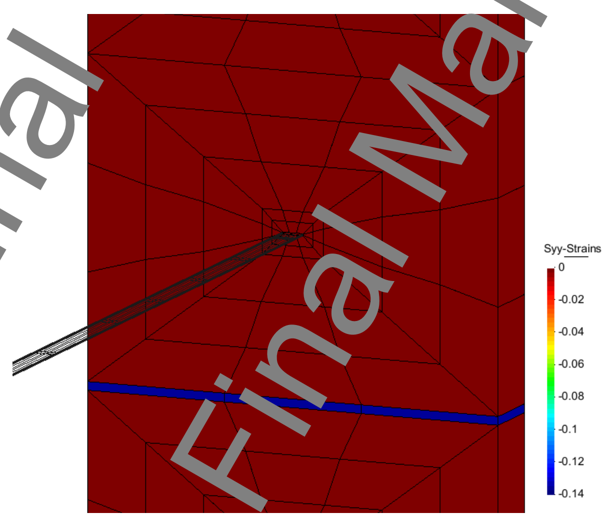

Figure S4. Vertical and horizontal panel stresses developed at the end of construction in second panel from bottom of the wall and vertical strains (steel strip wall - Case 0).

Table S1. Parameters used to simulate PWRI wall (from **Yu et al. 2015a**)

Parameter	Value
Concrete unit weight γ_c (kN/m^3)	24.0 [(a)]
Elastic modulus E_c (GPa)	32.0
Panel width (m)	0.18
Backfill peak plane strain friction angle, ϕ (°)	44
Backfill cohesive strength, c (kPa)	1
Backfill dilatancy angle, ψ (°)	14
Backfill unit weight, γ (kN/m^3)	18
Backfill stiffness, E_b (MPa)	20
Backfill stiffness, $E_{b(1st\text{-}m)}$ (MPa)	10
Poisson's ratio, v (-)	0.45
Foundation peak plane strain friction angle, ϕ (°)	36
Foundation cohesive strength, c (kPa)	1
Foundation dilatancy angle, ψ (°)	6
Foundation backfill unit weight, γ (kN/m^3)	18
Foundation stiffness, E_f (MPa)	13.5
Poisson's ratio, v (-)	0.45
Bearing pad cross-sectional area (m^2/m length of wall)	0.0126
Bearing pad stiffness, E_p (MPa)	6.[illegible]
Bearing pad unit weight γ (kN/m^3)	10
Reinforcement stiffness, J_r (MN/m)	68.2
Global reinforcement stiffness, S_g (MPa)	61
Soil-facing interface strength-stiffness reduction factor, R_i (-)	0.67 [(b)]
Interface element stiffness, (MPa)	20
Interface element stiffness friction angle, δ [(b)] (°)	32.9
Soil-facing interface adhesion, c_a (kPa)	0.6
Soil-reinforcement pullout friction factor, F^* (-)	Variable: 1.8 at top of wall, decreasing to 0.6 at 3 m below crest of wall, and then constant thereafter

Notes:

[(a)] Unit weight of concrete in numerical model was increased by a factor of 0.180/0.150 to account for the wider panel width (180 mm) in the physical wall and the Yu et al. model, and the narrower panel width (150 mm) used for the numerical PWRI wall in the current study.

[(b)] Applied to backfill soil only to calculate modulus of soil-facing stiffness, adhesion and interface soil friction angle.

[(c)] The equivalent steel modulus for the steel strips in the PWRI wall using the same width and thickness of the steel strips in **Figure 2b** is E = 272.6 GPa.

END